RFI RETE FERROVIARIA ITALIANA
GRUPPO FERROVIE DELLO STATO ITALIANE

APPALTATORE A.T.I.

TOTO COSTRUZIONI GENERALI (Capogruppo Mandataria)

| | |
|---|---|
| ITALIANA COSTRUZIONI S.p.A. | (Mandante) |
| ESIM S.r.l. | (Mandante) |
| ALPITEL S.p.A. | (Mandante) |
| ARMAFER del Dr. Michele Morelli S.r.l. | (Mandante) |

**LINEA PALERMO-MESSINA RADDOPPIO FIUMETORTO-CEFALÙ-CASTELBUONO**
**TRATTA OGLIASTRILLO-CASTELBUONO**

## PROGETTO COSTRUTTIVO

# • RELAZIONE GEOLOGICA SITI DI PRODUZIONE E DESTINAZIONE TRS
# • RELAZIONE MARINE AND PETROLEUM GEOLOGY

Codice Elaborato

| COMMESSA | LOTTO | FASE | ENTE | OPERA | DISCIPLINA | TIPO | PROGR. | REV. |
|---|---|---|---|---|---|---|---|---|
| RS01 | 20 | C | ZZ | RHIM | 00 | 03 | 014 | A |

Scala: -

File: RS0120CZZRHIM0003014A.pdf

Formato: pdf -

| Rev, | Data | Descrizione | Redatto | Verificato | Approvato |
|---|---|---|---|---|---|
| A | Giugno 2021 | RELAZIONE GEOLOGICA & MARINE AND PETROLEUM | | | |
| | | | | | |
| | | | | | |
| | | | | | |
| | | | | | |

PROGETTAZIONE:

APPROVAZIONI:

COSTRUZIONI GENERALI

*Viale Abruzzo, 410 66100 CHIETI (CH)*

# STUDIO GEOLOGICO-STRUTTURALE DEL COMPRENSORIO INTERESSATO DALLA REALIZZAZIONE DELLE GALLERIE DIRADDOPPIO DEL TRACCIATO FERROVIARIO DELLA TRATTA CEFALU' OGLIASTRILLO – CASTELBUONO E DEI SITI DI DESTINAZIONEDELLE TERRE E ROCCE DI SCAVO

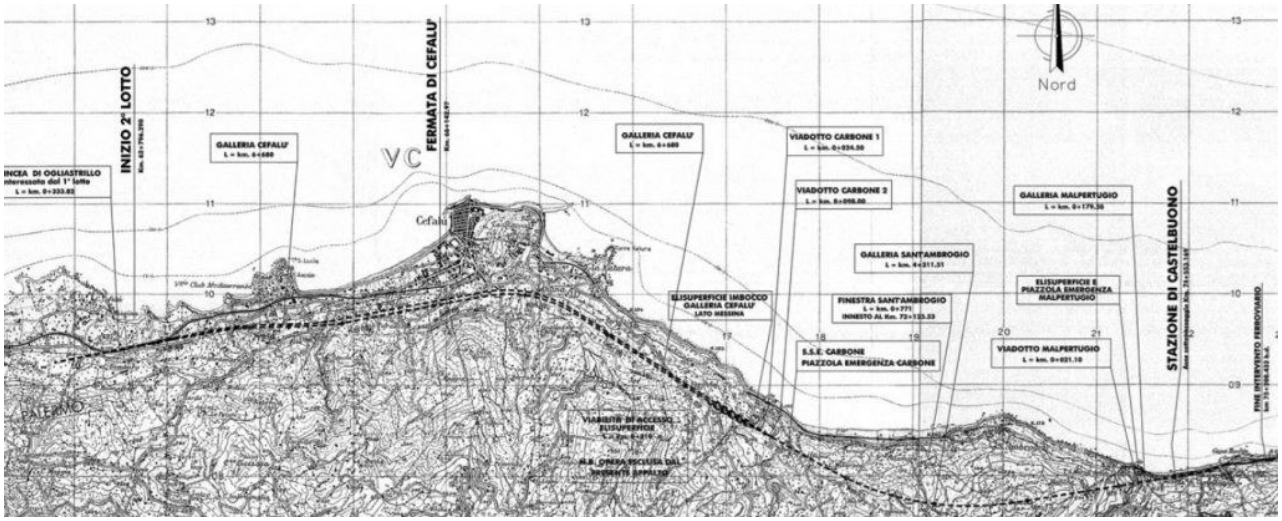


| ELABORATO | DATA |
|---|---|
| **Relazione geologica** | **14 giugno 2021** |

**Il consulente geologo**
Geol. Gian Vito Graziano

**Il Direttore Tecnico della ditta**
Ing. Giovanni Pinna

*Studio Geologico G. Graziano e M. Masi – Via Aquileia, 34/ 90144 Palermo mail: grazianoemasi@gmail.com*

INDICE

## 1. PREMESSA

Il Raggruppamento Temporaneo di Imprese (RTI), di cui la *Toto S.p.A. Costruzioni Generali* di Chieti è mandataria, è appaltatore dei lavori di costruzione del raddoppio ferroviario della tratta Ogliastrillo-Castelbuono della linea Palermo-Messina. Si tratta di un tracciato ferroviario che dalla località Ogliastrillo, a Ovest di Cefalù, si sviluppa per circa 12,3 km, quasi tutto in galleria, sino alla stazione di Castelbuono.

Più dettagliatamente è prevista la realizzazione di tre gallerie naturali di linea, intervallate da brevi tratti allo scoperto:

1. Galleria *Cefalù*, a doppia canna, dello sviluppo di circa 7 km.
2. Galleria *S. Ambrogio*, a singola canna, lunga circa 4 km,
3. Galleria *Malpertugio*, a singola canna, lunga 180 m circa

I brevi tratti allo scoperto sono collocati alle estremità dell'intervento, in località Ogliastrillo e nel tratto interessato dalla stazione di Castelbuono e in corrispondenza delle incisioni dei torrenti Mazzatore e Carbone, tra le gallerie *Cefalù* e *S. Ambrogio*, e del Torrente Malpertugio, tra le gallerie *S. Ambrogio* e *Malpertugio*.

Sono previsti ulteriori lavori in sotterraneo a servizio della fermata sotterranea di Cefalù, che si sviluppa lungo l'omonima galleria, e la galleria finestra S. Ambrogio, per la gestione delle emergenze della galleria di linea S. Ambrogio.

Il tracciato si snoda parallelamente alla linea di costa, interessando una fascia di terreni le cui quote altimetriche variano da circa m 30,00 ad oltre m 300,00 s.l.m.

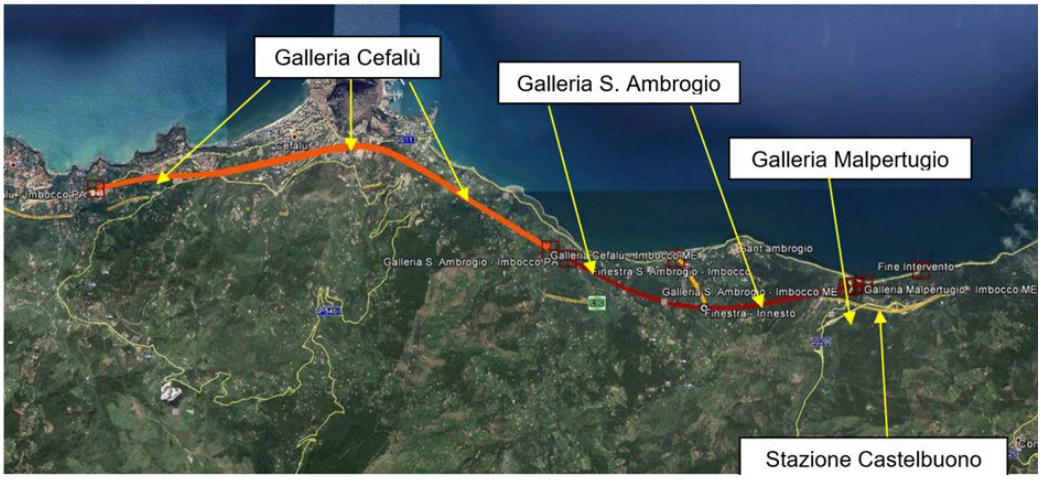


***Fig. 1: sviluppo del raddoppio ferroviario***

Per i riferimenti topografici esso ricade in parte nel Foglio n. 597130 e in parte nel Foglio n 597140 della Cartografia Tecnica Regionale (CTR) della Sicilia in scala 1:10.000.

L'Appaltatore è soggetto produttore del materiale da scavo, nonché proponente ed esecutore del Piano di utilizzo predisposto ai sensi del D.M. 161/12, che è stato approvato della Direzione Generale per le Valutazioni e Autorizzazioni Ambientali del Ministero dell'Ambiente - MATTM (determina DVADEC-2015-0000206 del 22 giugno 2015 e Decreto Direttoriale n. 470/DVA.29.12.2016).

Nel corso delle attività di caratterizzazione dei materiali prelevati mediante sondaggio alla profondità del cavo delle gallerie, effettuate in ottemperanza alle prescrizioni contenute nel provvedimento di approvazione del Piano di Utilizzo, e delle attività preliminari di caratterizzazione ambientale di potenziali siti di destinazione finale dei materiali da scavo, sono state riscontrate frequenti concentrazioni di idrocarburi pesanti (C >12) che superano le Concentrazioni Soglia di Contaminazione (CSC) di cui alla colonna A, Tabella 1, Allegato 5, Titolo V, Parte IV, del Decreto Legislativo n. 152 del 3 aprile 2006. 2006, ancorché largamente inferiori alla soglia di 750 mg/kg indicata in colonna B.

Tali superamenti sono stati riscontrati anche nella caratterizzazione dei materiali da scavo prelevati dal cavo delle gallerie in fase di esecuzione e mediante sondaggi orizzontali al fronte. Le concentrazioni misurate attingono valori fino a 258 mg/kg.

Valutazioni sulla frequenza dei rilevamenti, sulla giacenza dei punti di prelievo e sugli esiti analitici di speciazioni MADEP hanno avvalorato l'ipotesi che la presenza rilevata degli idrocarburi pesanti e le relative concentrazioni misurate siano da attribuire alla presenza di frazioni di sostanza organica di origine biogena negli orizzonti profondi della formazione geologica affiorante ed entro la quale sono stati eseguiti i prelievi costituendo, quindi, una caratteristica di fondo naturale di questi terreni.

Nell'ipotesi di utilizzo del materiale scavato in un sito diverso rispetto a quello di produzione, l'utilizzo stesso deve riguardare un ambito territoriale con fondo naturale con caratteristiche analoghe e confrontabili per tutti i parametri oggetto di superamento nella caratterizzazione del sito di produzione.

L'Appaltatore ha pertanto provveduto a comunicare all'ARPA territorialmente competente e al Ministero dell'Ambiente e della Tutela del Territorio e del Mare, Autorità Competente il rilevamento dei superamenti della CSC di col. A, Tabella 1, Allegato 5, Titolo V, Parte IV, del Decreto Legislativo n. 152 del 3 aprile 2006 e ha predisposto e trasmesso agli stessi Enti i piani di indagine per l'accertamento dei valori di fondo naturale, che hanno riguardato sia il sito di produzione, sia i due siti di destinazione individuati, denominati rispettivamente "Luogo Marchese", sede di un progetto di rimodellamento, e "Roccalupa", una ex-cava oggetto di apposito progetto di recupero ambientale. Si rimanda all'esame di quei documenti per la descrizione delle indagini svolte.

## 2. INQUADRAMENTO GEOLOGICO

Il contesto geologico in seno al quale è prevista la realizzazione del tracciato ferroviario Cefalù Ogliastrillo – Castelbuono è rappresentato quasi esclusivamente dalla formazione oligo-miocenica del *Flysch Numidico*, solo a tratti mascherata in superficie dai depositi detritici e alluvionali di età olocenica di spessori generalmente modesti.

Si tratta della formazione maggiormente rappresentata, ben oltre i limiti del comprensorio strettamente interessato dai lavori, affiorando diffusamente, praticamente senza soluzione di continuità, dall'abitato di Cefalù ad Ovest sino a Castel di Tusa ad Est, per poi estendersi per decine di chilometri a monte in seno all'area madonita. E' costituita da depositi clastico-terrigeni di origine torbiditica di elevato spessore, formati in prevalenza da argilliti e argille variamente sabbiose di colore bruno tabacco, cui si alternano quarzareniti, talora grossolane, organizzate in strati e banchi. La successione è sostanzialmente formata da argilliti nerastre a stratificazione indistinta nella parte basale, passanti verso l'alto a una sottile alternanza di argilliti nerastre, quarzosiltiti di colore ocra e argille brune.

Sono diverse le carte geologiche del comprensorio che possono essere consultate: sempre redatte in ambito universitario, esse attribuiscono unanimemente i terreni presenti alla formazione del *Flysch Numidico*. In questa trattazione si è preferito fare riferimento al Foglio

"Cefalù-Castelbuono" e al limitrofo "Capo Plaia-Termini Imerese" della Carta Geologica d'Italia, redatta da ISPRA (progetto CARG), perché univocamente ritenuta la cartografia geologica ufficiale dello Stato italiano. In essa la formazione del *Flysch Numidico* è associata ad una delle unità geologiche più significative per spessore ed estensione, ossia al cosiddetto "*Membro di Geraci Siculo"*, attribuibile dal punto di vista stratigrafico all'intervallo *Oligocene superiore- Miocene inferiore*, il cui spessore si aggira tra i 400 e gli 800 metri.

Si vedrà infatti che la formazione è smembrata in grandi scaglie che hanno dato origine a distinte unità tettoniche, una della quali è rappresentata proprio dal "*Membro di Geraci Siculo*", che nel comprensorio studiato è fortemente interessato da una tettonica neogenica distensiva, che dà luogo a diversi sistemi di faglie, il più importante dei quali possiede orientamento prevalente NW-SE, come si osserva nello schema tettonico di *Fig. 2*.

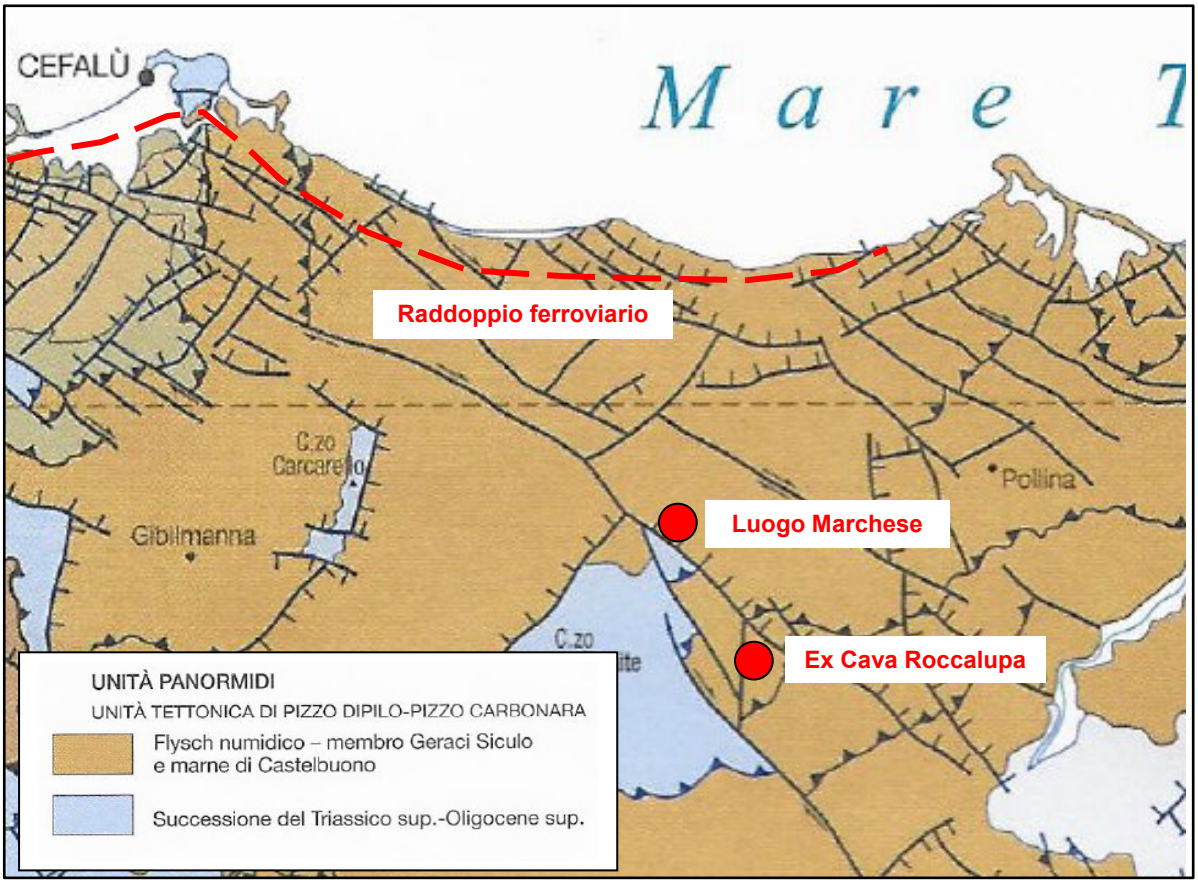


***Fig. 2: schema tettonico dell'area***

In seno ai termini prevalentemente argillosi del dal "*Membro di Geraci Siculo*", dunque all'interno della stessa formazione del *Flysch Numidico*, si trovano il sito di produzione del

materiale da scavo (gallerie) e i due siti di destinazione del materiale scavato, ossia l'ex cava Roccalupa e il cosiddetto "Luogo Marchese", entrambi in agro di Pollina.

Il sito di destinazione finale della ex Cava Roccalupa si trova a circa 6 Km a monte dallo sviluppo del raddoppio ferroviario, a una quota compresa tra 270 e 380 m s.l.m., mentre il sito di Luogo Marchese si trova a circa 1,5 mm a Nord-Ovest, in un contesto di pressoché totale assenza di urbanizzazione, fatti salvi strade ed edifici sparsi con carattere rurale. Va precisato che la ex Cava Roccalupa si trova in seno a un modesto affioramento di calcari di scoglieradi età Giurassica ("*Calcari di Piano Battaglia*"), presenti sul lato rialzato di una faglia diretta e contornati per buona parte dalle argille del *Flysch Numidico* e sul solo lato occidentale della faglia, ossia sul suo lato ribassato, dalla formazione argillosa delle *Marne di Castelbuono*, in continuità di sedimentazione sopra lo stesso *Flysch Numidico*.

Completano il quadro geologico i terrazzi marini presenti ad Ovest di Cefalù, dove interessano le aree prossime alla linea di costa, che tuttavia non sono interessati dallo sviluppo delle gallerie.

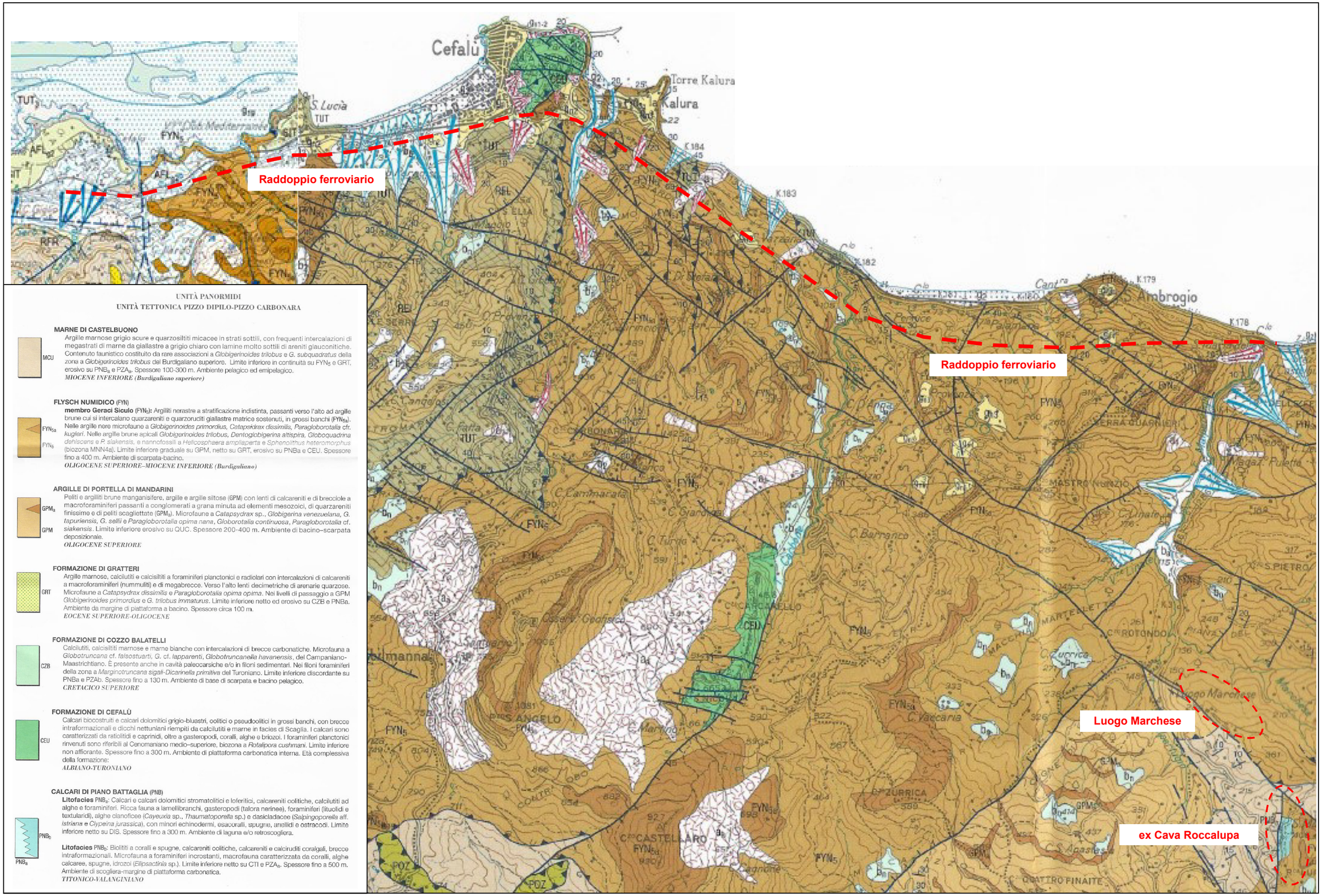


*Fig. 3: stralcio della Carta Geologica d'Italia – Foglio 596 -609 Capo Plaia-Termini Imerese a sinistra e Foglio 597-610 Cefalù-Castelbuono a destra*

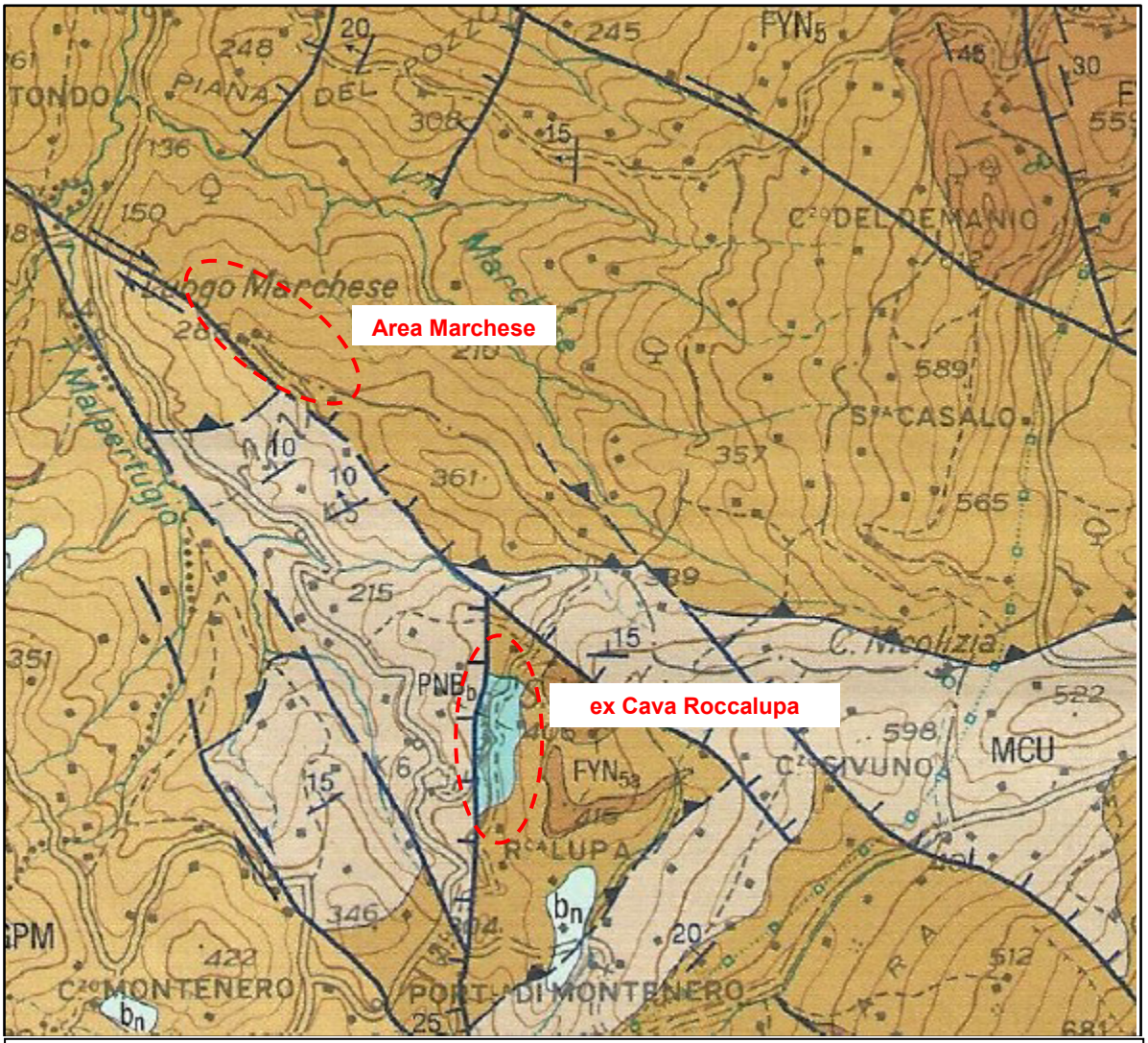


**FLYSCH NUMIDICO** (FYN)

**membro Geraci Siculo** ($FYN_5$)**:** Argilliti nerastre a stratificazione indistinta, passanti verso l'alto ad argille brune cui si intercalano quarzareniti e quarzoruditi giallastre matrice sostenuti, in grossi banchi ($FYN_{5a}$). Nelle argille nere microfaune a *Globigerinoides primordius, Catapsidrax dissimilis, Paragloborotalia* cfr. *kugleri*. Nelle argille brune apicali *Globigerinoides trilobus, Dentoglobigerina altispira, Globoquadrina dehiscens* e *P. siakensis*, e nannofossili a *Helicosphaera ampliaperta* e *Sphenolithus heteromorphus* (biozona MNN4a). Limite inferiore graduale su GPM, netto su GRT, erosivo su PNBa e CEU. Spessore fino a 400 m. Ambiente di scarpata-bacino.

*OLIGOCENE SUPERIORE–MIOCENE INFERIORE (Burdigaliano)*

$FYN_{5a}$

$FYN_5$

**CALCARI DI PIANO BATTAGLIA** (PNB)

**Litofacies** $PNB_a$: Calcari e calcari dolomitici stromatolitici e loferitici, calcareniti oolitiche, calcilutiti ad alghe e foraminiferi. Ricca fauna a lamellibranchi, gasteropodi (talora nerinee), foraminiferi (lituolidi e textularidi), alghe cianoficee (*Cayeuxia* sp., *Thaumatoporella* sp.) e dasicladacee (*Salpingoporella* aff. *istriana* e *Clypeina jurassica*), con minori echinodermi, esacoralli, spugne, anellidi e ostracodi. Limite inferiore netto su DIS. Spessore fino a 300 m. Ambiente di laguna e/o retroscogliera.

$PNB_b$

$PNB_a$

**Litofacies** $PNB_b$: Biolititi a coralli e spugne, calcareniti oolitiche, calcareniti e calciruditi coralgali, brecce intraformazionali. Microfauna a foraminiferi incrostanti, macrofauna caratterizzata da coralli, alghe calcaree, spugne, idrozoi (*Ellipsactinia* sp.). Limite inferiore netto su CTI e $PZA_a$. Spessore fino a 500 m. Ambiente di scogliera-margine di piattaforma carbonatica.

*TITONICO-VALANGINIANO*

***Fig. 4: stralcio della Carta Geologica d'Italia - Foglio "Cefalù-Castelbuono" Progetto CARG, ISPRA, ingrandito alla scala 1:25.000***

## 3. LE INDAGINI SVOLTE

*3.1 Carotaggi e litostratigrafie*

Nella fase di caratterizzazione ambientale del tracciato ferroviario furono eseguiti diversi sondaggi verticali (tra il 2013 e il 2016), di cui diversi spinti sino al cavo delle gallerie principali di progetto (profondità massima di poco inferiore a 100 metri dal piano di campagna), nel corso dei quali furono prelevati a profondità variabili alcune decine di campioni poi sottoposti ad analisi chimiche.

In numerosissimi campioni fu accertata la presenza di sostanze idrocarburiche (analiticamente determinate come "*Idrocarburi pesanti C10-C40*"), con concentrazioni che in diversi casi superavano il valore limite tabellare di 50 mg/kg (colonna A).

Ulteriori indagini preliminari espletate successivamente mediante sondaggi sia sul sito di produzione (sondaggi orizzontali ai fronti delle gallerie), che su uno dei siti di destinazione, hanno condotto ad analoghi esiti analitici.

Rimandando, per maggiori dettagli, ai Piani di Accertamento predisposti e attuati dal proponente, essi hanno comportato l'esecuzione delle indagini che, di seguito, si sintetizzano:

Per il sito di produzione:

- 4 sondaggi orizzontali, due in corrispondenza dei fronti – lato Palermo e lato Messina - della galleria *S. Ambrogio*, verso l'interno della stessa, uno al fronte della galleria denominata *Finestra S. Ambrogio* e uno all'imbocco della galleria Cefalù, lato Messina;
- 4 sondaggi verticali in corrispondenza degli imbocchi di accesso agli stessi fronti delle gallerie.

I quattro sondaggi orizzontali si sono prolungati per 40 metri lineari verso l'interno delle gallerie, mentre i sondaggi verticali hanno raggiunto profondità variabili tra m 20,00 e m 23,00 dal piano di campagna agli imbocchi delle stesse gallerie.

Per quanto riguarda i siti di destinazione: dei materiali da scavo, nell'area dell'ex Cava Roccalupa sono stati eseguiti 12 sondaggi verticali, tutti spinti sino alla profondità di m 20,00

dal piano di campagna; nel sito denominato “Luogo Marchese” sono stati invece eseguiti 18 sondaggi verticali, anch’essi spinti sino alla profondità di 20,00 dal piano di campagna.

Tutti i sondaggi, con riferimento sia ai siti di produzione, sia a quelli di destinazione, sono stati eseguiti in seno alla formazione del *Flysch Numidico* e specificatamente alla sua unità Membro di Geraci Siculo.

Con riferimento al sito di produzione, i sondaggi verticali S1 e S2 eseguiti agli imbocchi della galleria *S. Ambrogio*, rispettivamente lato Palermo e lato Messina, hanno permesso di ricavare una litostratigrafia abbastanza semplice e uniforme, costituita da un orizzonte superiore formato da argille debolmente sabbiose, sopra un substrato di argilliti.

Questa sostanziale uniformità litologica è confermata dai sondaggi orizzontali eseguiti al fronte lato Palermo (S03-GN05) e al fronte lato Messina (S04-GN05), dove si riscontrano quasi esclusivamente argilliti.

Il sondaggio verticale S4, eseguito all’imbocco della galleria *finestra S. Ambrogio* lato Messina, mette in evidenza una litostratigrafia formata esclusivamente de sabbie argillose, mentre il sondaggio orizzontale (S02-GN06), eseguito al fronte della galleria verso l’interno, conferma la presenza, in questo caso esclusiva, delle argilliti.

Il sondaggio verticale S3, infine, eseguito in località Ogliastrillo (sulla SS113, in prossimità del Palazzetto dello Sport), poco distante dall’imbocco lato Palermo della galleria *Cefalù*, fa rilevare ancora un orizzonte superiore formato da argille debolmente sabbiose, stavolta poggiante sopra un substrato eterogeneo di sabbie limose, limi sabbiosi e limi argillosi tra loro alternati.

Il sondaggio orizzontale (S01-GI05), eseguito all’imbocco della galleria *Cefalù*, ma sul lato Messina, conferma questa eterogeneità, intercettando in successione verso l’interno prima delle argille ghiaiose debolmente sabbiose, poi argilliti, quarzosiltiti e quarzareniti.

Situazioni litologiche del tutto comparabili, pur nella loro eterogeneità, con quelle riscontrate nel sito di produzione si sono riscontrate nei siti di destinazione.

Nel sito Luogo Marchese si è evidenziato un orizzonte superficiale formato da argille debolmente sabbiose, localmente interrotte dalla presenza di elementi lapidei quarzarenitici, sopra un orizzonte basale di argille e/o argilliti grigie.

Maggiore eterogeneità litologica è stata riscontata nei sondaggi eseguiti nell'area dell'ex cava Roccalupa, sul lato rialzato della faglia diretta che lambisce l'area e che ha "sollevato" tettonicamente i *Calcari di Piano Battaglia* un tempo estratti nella stessa cava: i sondaggi hanno ancora riguardato i terreni del *Membro di Geraci Siculo*, dunque la formazione geologica del *Flysch Numidico*, ma con litologie prevalenti di argille sabbiose, oltre alle solite quarzareniti.

E' importante sottolineare che solo in tre di questi sondaggi è stata rilevata la presenza di acqua sotterranea a pelo libero: nel sondaggio S03 (Galleria Cefalù) alla profondità di m 12,46 dal p.c., nel sondaggio S18 nel sito Luogo Marchese alla profondità di m 14,21 dal p.c. e nel sondaggio S11 del sito dell'ex Cava Roccalupa alla profondità di m 9,18 dal p.c.

I tre fori di sondaggio sono stati attrezzati a piezometro.

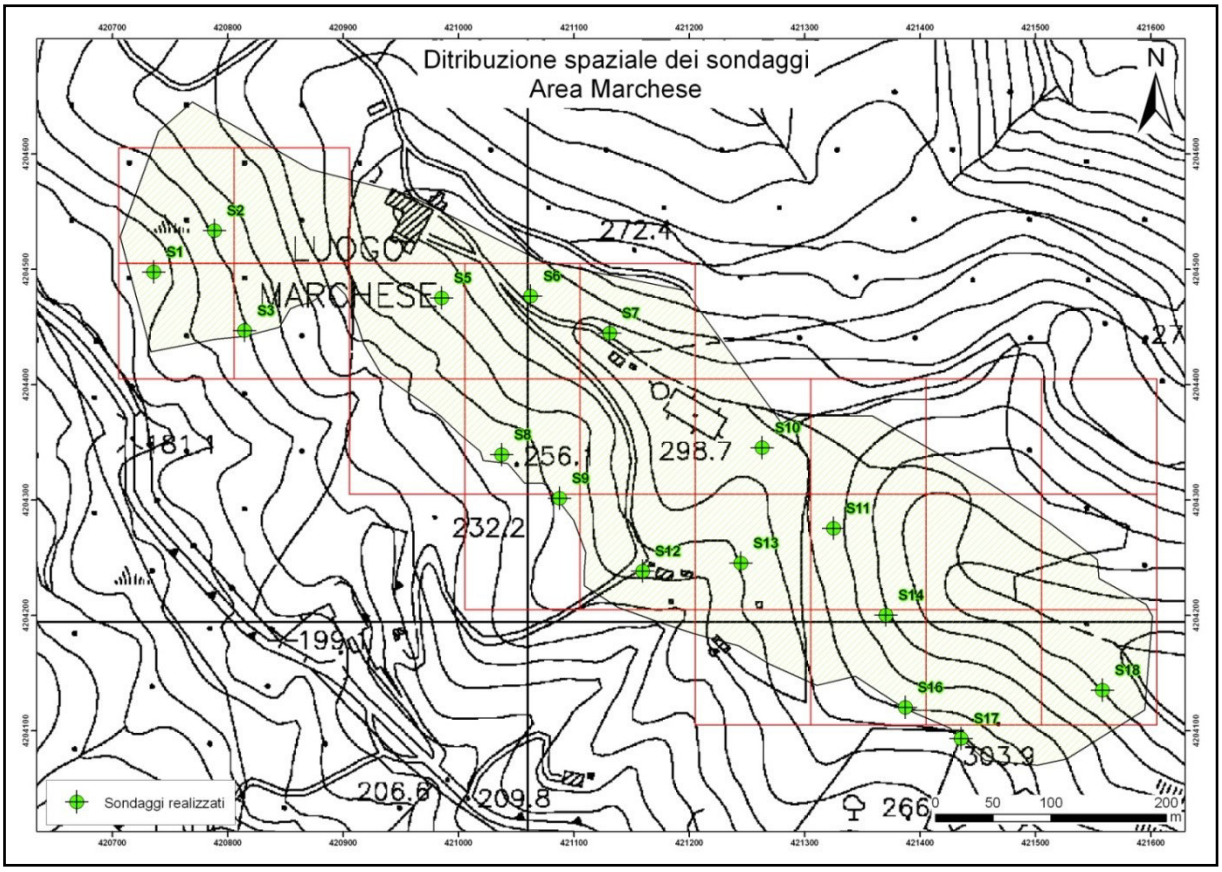


***Fig. 5: sondaggi eseguiti nel sito Luogo Marchese***

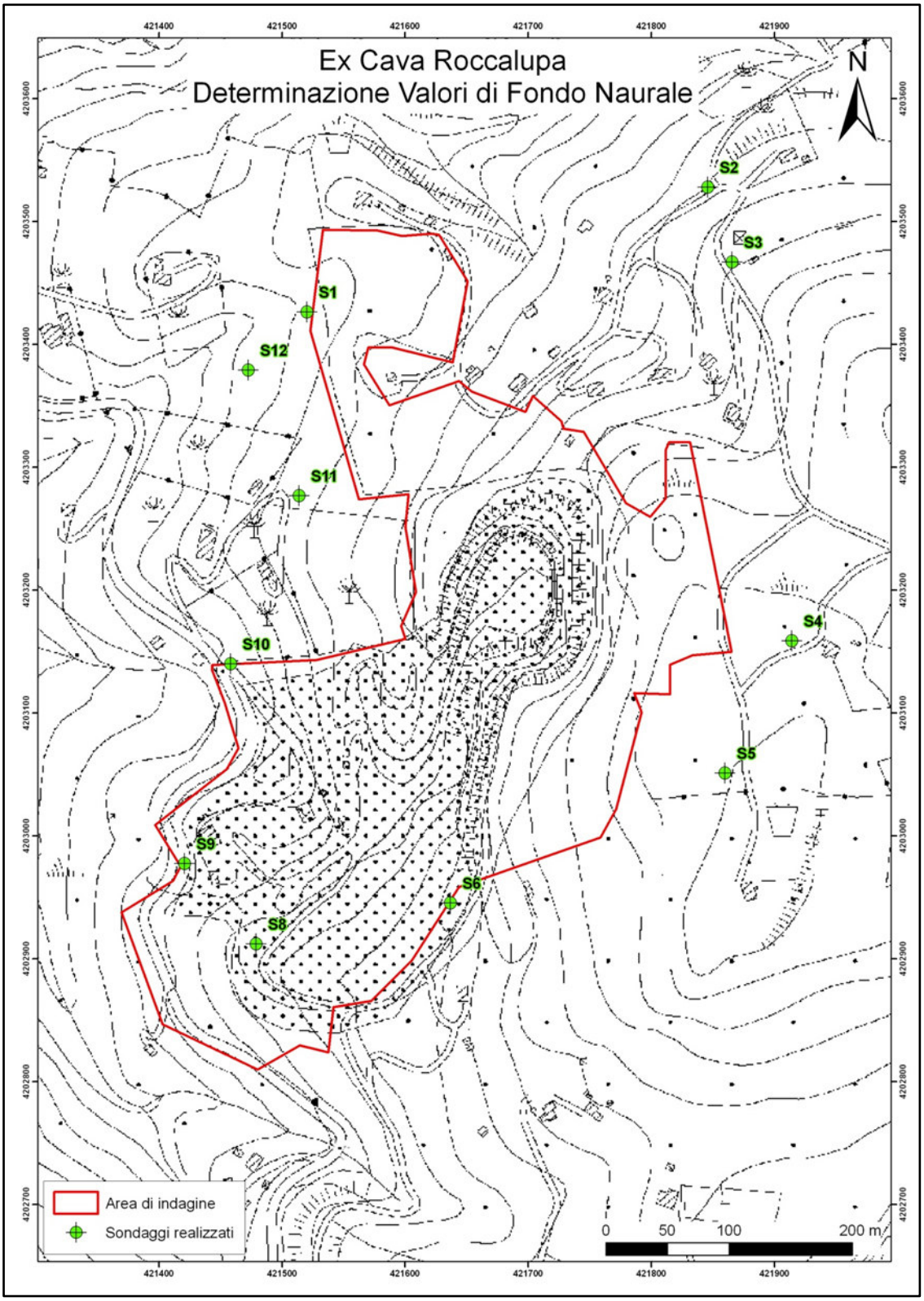


*Fig. 6: sondaggi eseguiti nell'area della ex Cava Roccalupa*

*3.2 Campioni prelevati e analisi*

Nell'ambito dell'attuazione del piano di accertamento dei valori di fondo naturale nel sito si produzione, sono stati prelevati 12 campioni nel corso dei 4 sondaggi verticali e ulteriori 16 campioni nel corso dei 4 sondaggi orizzontali.

Nei due siti di destinazione 36 campioni hanno riguardato l'area dell'ex Cava Roccalupa, 48 campioni hanno riguardato il sito di Luogo Marchese.

Rimandando per maggiore dettaglio e per un più autorevole commento dei risultati analitici alle relazioni redatte dal laboratorio CADA che ha eseguito la caratterizzazione, si espongono di seguito alcune considerazioni rapportate al contesto geologico locale, che consentono di inquadrare proprio in quel contesto i risultati analitici di cui alle attività di caratterizzazione

Praticamente quasi tutti i campioni presi in considerazione, prelevati a profondità variabili nei sondaggi verticali e a distanze variabili dagli imbocchi delle gallerie nei sondaggi orizzontali, presentano una componente di idrocarburi pesanti C > 12, in concentrazioni diverse, che in qualche caso superano i 200 mg/kg. Sono interessate da queste concentrazioni di idrocarburi tutte le facies litologiche riscontrate attraverso i sondaggi.

| Sondaggio | Campione | Profondità (m) | C > 12 (mg/kg) | Litologia |
|---|---|---|---|---|
| S1-GN05-PA (S.Ambrogio lato PA) | C1 | 2 -3 | 22 | Argille debolmente sabbiose |
| S1-GN05-PA (S.Ambrogio lato PA) | C2 | 9 - 10 | 55 | Argille debolmente sabbiose |
| S1-GN05-PA (S.Ambrogio lato PA) | C3 | 21 - 22 | 40 | Argilliti consistenti |
| S2-GN05-ME (S.Ambrogio lato ME) | C1 | 1 - 2 | 60 | Argille debolmente sabbiose |
| S2-GN05-ME (S.Ambrogio lato ME) | C2 | 9 - 10 | 108 | Argilliti consistenti |
| S2-GN05-ME (S.Ambrogio lato ME) | C3 | 19 - 20 | 187 | Argilliti consistenti |
| S3-GI01-PA (Cefalù lato PA) | C1 | 4 - 5 | 0 | Argille sabbiose |
| S3-GI01-PA (Cefalù lato PA) | C2 | 7,5 - 8 | 28 | Argille sabbiose |
| S3-GI01-PA (Cefalù lato PA) | C3 | 11,7 - 12 | 26 | Argille sabbiose |
| S4-GN06-fin.S.AMBR. (fin. S.Ambrogio lato ME) | C1 | 0 - 1 | 113 | Terre di riporto prevalentemente argillose provenienti dalla stessa formazione |
| S4-GN06- fin S.AMBR. (fin. S.Ambrogio lato ME) | C2 | 9 - 10 | 56 | Sabbie argillose |
| S4-GN06- fin. S.AMBR. (fin. S.Ambrogio lato ME) | C3 | 19 - 20 | 62 | Sabbie argillose |

***Fig. 7: tabella riassuntiva dei campioni dei sondaggi verticali presso il sito di produzione***

Come si osserva analizzando più attentamente i valori delle concentrazioni, non si riscontra alcun rapporto lineare sia nell'associazione tra litofacies e concentrazioni, sia in quella tra profondità e concentrazioni.

Valori di concentrazione variabili tra 0 e 60 mg/kg si sono misurate in seno alle argille sabbiose, tra 56 e 62 mg/kg in seno alle sabbie argillose e tra 40 e 187 mg/kg nelle argille consistenti e nelle argilliti.

Analizzando l'associazione tra profondità e concentrazioni, si è constatato che solo nel sondaggio S2-GN02-ME (S. Ambrogio lato Messina) le concentrazioni aumentano all'aumentare della profondità, mentre negli altri sondaggi esse variano irregolarmente talora in aumento, talaltra in diminuzione, persino all'interno della stessa verticale di sondaggio.

Considerazioni analoghe valgono per i sondaggi orizzontali, anche se in questi ultimi la diversità litologica è meno accentuata, prevalendo in larga misura le argilliti e le argille scagliettate, con concentrazioni variabili tra 46 e 192 mg/kg.

Valori compresi tra 38 e 91 mg/kg si riscontrano per le porzioni rocciose quarzarenitiche.

Nell'analisi dei rapporti tra distanza dall'imbocco e concentrazioni, si è constatato che solo nel sondaggio S03-GN05-PA (S. Ambrogio lato Palermo) le concentrazioni diminuiscono all'aumentare della distanza, mentre negli altri sondaggi esse variano ancora irregolarmente talora in aumento, talaltra in diminuzione all'interno della stessa orizzontale di sondaggio.

| Sondaggio | Campione | Profondità (m) | C > 12 (mg/kg) | Litologia |
|---|---|---|---|---|
| S02-GN06-fin.S.AMBR (fin. S.Ambrogio lato ME) | C1 | 0–1 | 181 | Argilliti consistenti |
| S02-GN06-fin.S.AMBR (fin. S.Ambrogio lato ME) | C2 | 9 – 10 | 190 | Argilliti consistenti |
| S02-GN06-fin.S.AMBR (fin. S.Ambrogio lato ME) | C3 | 19 - 20 | 150 | Argilliti consistenti |
| S02-GN06-fin.S.AMBR (fin. S.Ambrogio lato ME) | C4 | 29–30 | 155 | Argilliti consistenti |
| S02-GN06-fin.S.AMBR (fin. S.Ambrogio lato ME) | C5 | 39–40 | 166 | Argilliti consistenti |
| S04-GN05-ME (S.Ambrogio lato ME) | C1 | 0 – 1 | 120 | Argilliti consistenti |
| S04-GN05-ME (S.Ambrogio lato ME) | C2 | 9 – 10 | 91 | Argilliti e quarzareniti |
| S04-GN05-ME (S.Ambrogio lato ME) | C3 | 19 - 20 | 144 | Argilliti consistenti |
| S04-GN05-ME (S.Ambrogio lato ME) | C4 | 29 – 30 | 106 | Argilliti consistenti |
| S04-GN05-Me (S.Ambrogio lato ME) | C5 | 39 – 40 | 62 | Argilliti consistenti |

| | | | | |
|---|---|---|---|---|
| S01-GI05-ME (Cefalù lato ME) | C3 | 20 - 21 | 38 | Quarzarenite |
| S01-GI05-ME (Cefalù lato ME) | C4 | 29 – 30 | 46 | Argille ghiaiose debolmente sabbiose |
| S01-GI05-ME (Cefalù lato ME) | C5 | 39 – 40 | 123 | Argilliti consistenti |
| S03-GN05-PA (S.Ambrogio lato PA) | C3 | 20 - 21 | 192 | Argille scagliettate e argilliti |
| S03-GN05-PA (S.Ambrogio lato PA) | C4 | 29 – 30 | 110 | Argille scagliettate e argilliti |
| S03-GN05-PA (S.Ambrogio lato PA) | C5 | 39 – 40 | 76 | Argille scagliettate |

***Fig. 8: tabella riassuntiva dei campioni dei sondaggi orizzontali presso il sito di produzione***

Anche per i campioni prelevati nel corso dei sondaggi verticali nei due siti di destinazione non si riscontrano rapporti lineari univoci e costanti tra litofacies e concentrazioni e tra profondità e concentrazioni.

Al sito dell'ex Cava Roccalupa si sono misurati valori di concentrazione variabili tra 0 e 104 mg/kg in seno alle argille sabbiose e alle argille scagliettate, tra 48 e 53 mg/kg in seno alle argilliti e tra 26 e 183 mg/kg nelle quarzareniti. Al sito Luogo Marchese, in cui le argille sabbiose sono largamente predominanti, i valori di concentrazione misurati variano tra 0 e 207 mg/kg.

Analizzando l'associazione tra profondità e concentrazioni, a Cava Roccalupa si è constatato che solo nei sondaggi S1, S9 e S10 le concentrazioni aumentano all'aumentare della profondità, mentre negli altri sondaggi esse variano in maniera del tutto irregolare. Una maggiore linearità si rileva nei sondaggi eseguiti nel sito Luogo Marchese, dove le concentrazioni aumentano all'aumentare della profondità in S1, S2, S3, S7, S8, S9, S11, S12, S13, S14 e S18, mentre nei sondaggi S5 e S17 le concentrazioni diminuiscono all'aumentare della profondità e nei rimanenti variano irregolarmente.

| Sondaggio | Campione | Profondità (m) | C > 12 (mg/kg) | Litologia |
|---|---|---|---|---|
| S1 | C1 | 0 -1 | 40 | Argille debolmente sabbiose |
| S1 | C2 | 9 - 10 | 56 | Argille debolmente sabbiose |
| S1 | C3 | 19 - 20 | 83 | Argille debolmente sabbiose |
| S2 | C1 | 1 - 2 | 23 | Argille debolmente sabbiose |
| S2 | C2 | 9 - 10 | < 1 | Argille debolmente sabbiose |
| S2 | C3 | 19 - 20 | 25 | Argille debolmente sabbiose |
| S3 | C1 | 0 - 1 | 29 | Argille debolmente sabbiose |
| S3 | C2 | 9 - 10 | 26 | Argille debolmente sabbiose |
| S3 | C3 | 19 -20 | 69 | Quarzareniti |
| S4 | C1 | 0 - 1 | 46 | Argille debolmente sabbiose |

| | | | | |
|---|---|---|---|---|
| S4 | C2 | 9 - 10 | 26 | Quarzareniti |
| S4 | C3 | 19 - 20 | 183 | Quarzareniti |
| S5 | C1 | 0 - 3 | 27 | Argille debolmente sabbiose |
| S5 | C2 | 9 - 10 | 23 | Quarzareniti |
| S5 | C3 | 19 - 20 | 96 | Quarzareniti |
| S6 | C1 | 0 - 1 | 31 | Argille debolmente sabbiose |
| S6 | C2 | 9 -10 | < 1 | Argille debolmente sabbiose |
| S6 | C3 | 19 - 20 | 23 | Quarzareniti |
| S7 | C1 | 0 - 1 | 25 | Argille debolmente sabbiose |
| S7 | C2 | 9 - 10 | < 1 | Argille debolmente sabbiose |
| S7 | C3 | 19 - 20 | 48 | Argilliti consistenti |
| S8 | C1 | 0 - 1 | 51 | Argille debolmente sabbiose |
| S8 | C2 | 9 -10 | 40 | Argille debolmente sabbiose |
| S8 | C3 | 19 - 20 | 45 | Argille debolmente sabbiose |
| S9 | C1 | 1,5 – 2,5 | 56 | Argille debolmente sabbiose |
| S9 | C2 | 9 - 10 | 73 | Argille debolmente sabbiose |
| S9 | C3 | 19 - 20 | 123 | Argille scagliettate |
| S10 | C1 | 1,5–2,5 | < 1 | Argille debolmente sabbiose |
| S10 | C2 | 9 -10 | 104 | Argille debolmente sabbiose |
| S10 | C3 | 19 - 20 | 153 | Argilliti consistenti |
| S11 | C1 | 0 - 1 | 32 | Argille debolmente sabbiose |
| S11 | C2 | 9 - 10 | < 1 | Argille scagliettate |
| S11 | C3 | 19 - 20 | 48 | Argille scagliettate |
| S12 | C1 | 0 - 1 | < 1 | Argille debolmente sabbiose |
| S12 | C2 | 4 – 5 | < 1 | Argille debolmente sabbiose |
| S12 | C3 | 8 - 9 | < 1 | Argille debolmente sabbiose |

***Fig. 9: tabella riassuntiva dei campioni dei sondaggi verticali presso ex Cava Roccalupa***

| Sondaggio | Campione | Profondità (m) | C > 12 (mg/kg) | Litologia |
|---|---|---|---|---|
| S1 | C1 | 0 – 1 | 25 | Argille debolmente sabbiose |
| S1 | C2 | 9 – 10 | 56 | Argille debolmente sabbiose |
| S1 | C3 | 19 – 20 | 81 | Argille debolmente sabbiose |
| S2 | C1 | 0 – 1 | 57 | Argille debolmente sabbiose |
| S2 | C2 | 9 – 10 | 75 | Argille debolmente sabbiose |
| S2 | C3 | 19 – 20 | 81 | Argille debolmente sabbiose |
| S3 | C1 | 0 – 1 | 20 | Argille debolmente sabbiose |
| S3 | C2 | 9 – 10 | 21 | Argille debolmente sabbiose |
| S3 | C3 | 19 – 20 | 41 | Argille debolmente sabbiose |
| S5 | C1 | 0 – 1 | 207 | Argille debolmente sabbiose |
| S5 | C2 | 9 – 10 | 137 | Argille debolmente sabbiose |
| S5 | C3 | 19 – 20 | 129 | Argille debolmente sabbiose |
| S6 | C1 | 0 – 1 | 101 | Argille debolmente sabbiose |
| S6 | C2 | 9 – 10 | 65 | Argille debolmente sabbiose |
| S6 | C3 | 19 – 20 | 111 | Argilliti consistenti |
| S7 | C1 | 0 – 1 | 26 | Argille debolmente sabbiose |
| S7 | C2 | 9 – 10 | 72 | Argille debolmente sabbiose |
| S7 | C3 | 19 – 20 | 100 | Argille debolmente sabbiose |
| S8 | C1 | 0 – 1 | < 1 | Argille debolmente sabbiose |
| S8 | C2 | 9 – 10 | < 1 | Argille debolmente sabbiose |
| S8 | C3 | 19 – 20 | 76 | Argille debolmente sabbiose |
| S9 | C1 | 0 – 1 | 24 | Argille debolmente sabbiose |
| S9 | C2 | 9 – 10 | 32 | Argille debolmente sabbiose |
| S9 | C3 | 19 – 20 | 42 | Argille scagliettate |
| S10 | C1 | 0 – 1 | 30 | Argille debolmente sabbiose |
| S10 | C2 | 9 – 10 | 23 | Argille debolmente sabbiose |
| S10 | C3 | 19 – 20 | 24 | Argille debolmente sabbiose |

| | | | | |
|---|---|---|---|---|
| S11 | C1 | 0 – 1 | 20 | Argille debolmente sabbiose |
| S11 | C2 | 9 – 10 | 26 | Argille debolmente sabbiose |
| S11 | C3 | 19 – 20 | 39 | Argille scagliettate |
| S12 | C1 | 0 – 1 | 25 | Argille debolmente sabbiose |
| S12 | C2 | 9 - 10 | 130 | Argille debolmente sabbiose |
| S12 | C3 | 29 - 30 | 184 | Argille debolmente sabbiose |
| S13 | C1 | 0 – 1 | 28 | Argille debolmente sabbiose |
| S13 | C2 | 9 – 10 | 68 | Argille debolmente sabbiose |
| S13 | C3 | 19 – 20 | 94 | Argille debolmente sabbiose |
| S14 | C1 | 0 – 1 | < 1 | Argille debolmente sabbiose |
| S14 | C2 | 9 – 10 | 36 | Argille debolmente sabbiose |
| S14 | C3 | 19 – 20 | 59 | Argille debolmente sabbiose |
| S16 | C1 | 0 – 1 | 39 | Argille debolmente sabbiose |
| S16 | C2 | 9 – 10 | 49 | Argille debolmente sabbiose |
| S16 | C3 | 19 – 20 | 48 | Argille debolmente sabbiose |
| S17 | C1 | 0 – 1 | 49 | Argille debolmente sabbiose |
| S17 | C2 | 9 – 10 | 47 | Argille debolmente sabbiose |
| S17 | C3 | 19 – 20 | 36 | Argille debolmente sabbiose |
| S18 | C1 | 0 - 1 | 21 | Argille debolmente sabbiose |
| S18 | C2 | 2 - 3 | 30 | Argille debolmente sabbiose |
| S18 | C3 | 3 - 4 | 40 | Argille debolmente sabbiose |

***Fig. 10: tabella riassuntiva dei campioni dei sondaggi verticali presso il sito Luogo Marchese***

In definitiva i 112 campioni di terreno analizzati, 28 dei quali prelevati negli otto sondaggi al sito di produzione, 36 prelevati nei dodici sondaggi al sito dell'ex Cava Roccalupa e 48 prelevati nei diciotto sondaggi al sito Luogo Marchese, hanno fatto quasi sempre rilevare concentrazioni di C < 12 rilevabile strumentalmente (salvo che in 11 casi).

Esse spesso superano in 44 casi le CSC di cui alla colonna A, Tabella 1, Allegato 5, Titolo V, Parte IV, del Decreto Legislativo n. 152 del 3 aprile 2006. 2006, mantenendosi largamente sotto alla soglia di 750 mg/kg indicata in colonna B.

Non è stato possibile individuare correlazioni univoche tra le diverse concentrazioni di idrocarburi pesanti e le litofacies appartenenti alla formazione geologica del *Flysch Numidico* e specificamente a quelle afferenti all'unità definita *Membro di Geraci Siculo*

Allo stesso tempo non è stato possibile individuare correlazioni univoche tra le stesse concentrazioni e le profondità di prelievo dei campioni.

## 4. AMBIENTE DEPOSIZIONALE

*4.1 Bacino di sedimentazione*

Si è detto che l'origine della formazione flyschoide è torbiditica, ossia è formata da depositi clastico-terrigeni depositatisi lungo ampie scarpate deposizionali, in cui per gravità si sono sviluppati i flussi di torbida (*grain flow* e *debris flow*) che trasportavano materiale carbonatico e di conoide sottomarina.

Questi depositi hanno interessato aree talmente vaste da costituire la copertura terrigena delle successioni pelagiche del *Bacino Imerese*, dei sedimenti carbonatici della *Piattaforma Panormide* e persino di alcune successioni sedimentarie sicilidi originariamente più interne. In altre parole le dimensioni del loro bacino di sedimentazione è di scala regionale, con ampiezze dell'ordine di alcune centinaia di chilometri.

Si pensi che lo spessore massimo accertato per la formazione del *Flysch Numidico* è 1500 metri e che essa affiora estesamente dalla dorsale dei Nebrodi, al limite con la Catena Calabride, fino alle aree del trapanese.

Con specifico riferimento al comprensorio studiato, i termini flyschoidi affioranti lungo il tracciato ferroviario e nei due siti di destinazione delle terre e rocce provenienti dallo scavo delle gallerie, costituiscono la culminazione della dorsale affiorante in maniera estesa nelle Madonie, che rappresenta più precisamente la copertura discordante sopra una parte delle unità carbonatiche panormidi, rappresentate nell'area da calcari di età cretacica.

Sulla base di analisi sia di superficie che di sottosuolo, la letteratura geologica, a partire da Bianchi e*t alii* (1987), sostiene che questa formazione è disposta in grandi scaglie ripetute, scollate dal loro originario substrato mesozoico, che hanno dato origine a distinte diverse unità tettoniche. Ciò trova corrispondenza con l'attuale distribuzione della formazione, presente in affioramento per decine di chilometri e più volte duplicata tettonicamente fuori dal presente contesto territoriale, che consente di ricostruire un'originaria estensione, prima della deformazione, di aree vaste centinaia di chilometri.

Una di queste unità è rappresentata dal "*Membro di Geraci Siculo*", una successione terrigena di notevoli spessori, che si estende con uniformità geologica sia arealmente, sia in profondità

in tutto il comprensorio studiato sino a inglobare buona parte delle Madonie centro settentrionali. Gli enormi volumi da essa occupati sono molto più ampi di quelli, già cospicui, ipotizzabili sulla base dei dati di superficie.

In definitiva tutte le opere previste per il raddoppio ferroviario e i due siti di destinazione delle terre e rocce di scavo si sviluppano in seno a questa vasta unità tettonica, che costituisce un unico grande ambiente di deposizione.

*4.2 Materia organica nei sedimenti torbiditici*

Si forniscono in questo paragrafo alcune ulteriori informazioni acquisite da letteratura geologica, dalla quale emerge che la presenza degli idrocarburi C > 12 nella formazione geologica del *Flysch Numidico* sia di origine naturale e non antropica, associata alla presenza naturale di frazioni di sostanza organica di origine biogena negli orizzonti profondi della stessa formazione geologica.

Una prima ipotesi circa l'origine degli idrocarburi si lega al contesto geochimico in cui si inserisce la diagenesi del *Flysch Numidico*, ossia di rocce sedimentarie che traevano origine dalla disgregazione della litosfera e dal contestuale apporto di materiale biologico, come quello derivante dai fitodetriti depositati sul fondo del bacino di sedimentazione, che veniva poi intrappolato nelle correnti di torbida.

Studi sugli aspetti deposizionali e diagenetici delle argille del *Flysch Numidico* (*Dongarrà e Ferla*, 1982) convaliderebbero l'ipotesi che l'apporto terrigeno trovasse condizioni deposizionali caratterizzate da abbondante sostanza organica, che ne causava peraltro una diagenesi precoce.

La presenza di intercalazioni di livelli ad alto contenuto in ferro (*clayironstone*) confermerebbero la costante presenza di abbondante sostanza organica (Leone et alii, 1979; Calderone et alii, 1980). Le argomentazioni di alcuni autori sui dati composizionali della formazione, suffragate da dati isotopici sull'ossigeno e il carbonio, hanno portato infatti gli stessi autori a considerare la presenza abbondante di ferro, come risultato di una diagenesi

precoce avvenuta "*in un bacino chiuso ed evaporante….durante la decomposizione batterica di abbondante sostanza organica, della quale ancora sono visibili tracce residuali*".

Lo studio mineralogico e petrografico condotto Dongarrà e Ferla (1982) evidenzia che in tutti i campioni da loro sottoposti ad analisi erano state rinvenute piccole quantità di sostanza organica.

Una diagenesi precoce in bacini prevalentemente anossici potrebbe spiegare la conservazione della sostanza organica e allo stesso tempo la presenza degli idrocarburi formatisi per la trasformazione della stessa sostanza organica dispersa nelle rocce.

Una diversa interpretazione circa la presenza di idrocarburi in seno al *Flysch Numidico*, proprio nell'area compresa tra Cefalù e Castelbuono, viene data da alcuni studiosi belgi, danesi e inglesi (Dewever et alii - *Ricostruzione del flusso fluido nei calcari carsici della piattaforma Panormide - Sicilia centro-settentrionale: implicazioni per la prospettiva degli idrocarburi*, 2009) in uno studio basato su analisi diagenetiche, osservazioni di campo e petrografiche e dati isotopici, allegato in calce alla presente relazione. Secondo gli autori l'origine della presenza degli idrocarburi nell'area deve essere attribuita alla loro migrazione dai sottostanti calcari cretacei per la compressione tettonica da questi subita nel Miocene medio, ulteriormente favorita dalle successive faglie plioceniche.

Ricostruendo in cinque fasi tettoniche la storia dei flussi dei fluidi presenti nei calcari cretacei fortemente carsicizzati, essi indicano negli stessi calcari del dominio panormide la roccia madre in seno alla quale si sono formati bitume e fluorite, identificando gli stessi calcari presenti nelle Madonie come potenziale unità di giacimento di idrocarburi.

Lo studio si concentra su due distinti affioramenti rocciosi, a circa 15 km di distanza l'una dall'altra; il litorale roccioso appena a Nord della Rocca di Cefalù e la ex cava di Roccalupa, che, secondo la carta geologica presa a riferimento (Lentini e Vezzani, 1974), appartengono rispettivamente al Cretaceo superiore e al Cretaceo inferiore. Nella stessa carta i calcari di Roccalupa sono attribuiti alla *Formazione di Pizzo Canna*, solo successivamente classificati nel CARG come *Formazione di Piano Battaglia*. Entrambi gli affioramenti rappresentano differenti età stratigrafiche e sono caratterizzati anche da diversa sedimentologia, ma hanno

in comune un importante sistema carsico, in cui è abbondante la presenza di bitume, specialmente nei calcari di Roccalupa.

Il sistema carsico è meglio sviluppato appena sotto la discordanza tra i calcari cretacei e il superiore *Flysch Numidico*, dove è probabile che esistesse un sistema aperto che favoriva la migrazione degli idrocarburi durante le fasi compressive mioceniche

Nella *Fig. 11*, tratta dallo studio degli autori, viene rappresentata schematicamente la storia cinematica e fluidodinamica delle unità cretacee della *Piattaforma panormide* nella Sicilia centro-settentrionale dal Cretaceo ad oggi. Il disegno in alto a sinistra mostra l'inquadramento geologico nel Cretaceo con la piattaforma fiancheggiata dall'Oceano Ligure a Nord e dal Bacino Imerese a Sud. La sedimentazione nel dominio panormide durante il Cretaceo era eterogeneo e consisteva in una contemporanea sedimentazione pelagica e su piattaforme poco profonde. La sedimentazione pelagica prevalse nell'Oceano Ligure e nel Bacino Imerese con la risedimentazione di detriti carbonatici lungo i fianchi dell'alto strutturale della Piattaforma panormide. Il punto nero segna la generica collocazione dell'area di studio Cefalù-Castelbuono. Il disegno superiore mostra l'emersione di parte della piattaforma e la conseguente infiltrazione di acqua meteorica, responsabile del carsismo. Le frecce indicano i movimenti tettonici verticali che furono probabilmente la causa dell'emergenza. Il disegno al centro a sinistra è un ingrandimento del disegno precedente dove la piattaforma è nuovamente sommersa e rappresenta il momento in cui i sedimenti marini invadono il sistema carsico. Tornando al disegno a destra, questo rappresenta la sepoltura dell'avanfossa e la sedimentazione del *Flysch Numidico* nell'Oligocene-Miocene, contestualmente alla spinta compressiva che intanto è iniziata da Nord. Nel disegno in basso a sinistra la compressione avvenuta nel Miocene medio, mentre nell'ultima fase della storia del flusso, nel disegno in basso a destra, a seguito del sollevamento delle Madonie, il flusso del fluido è veicolato lungo le faglie che si sono sviluppate durante l'apertura del bacino di retroarco tirrenico.

Se l'ipotesi di espulsione di fluidi durante la compressione è corretta, l'area di origine dei fluidi era molto probabilmente localizzata a nord dell'area di studio

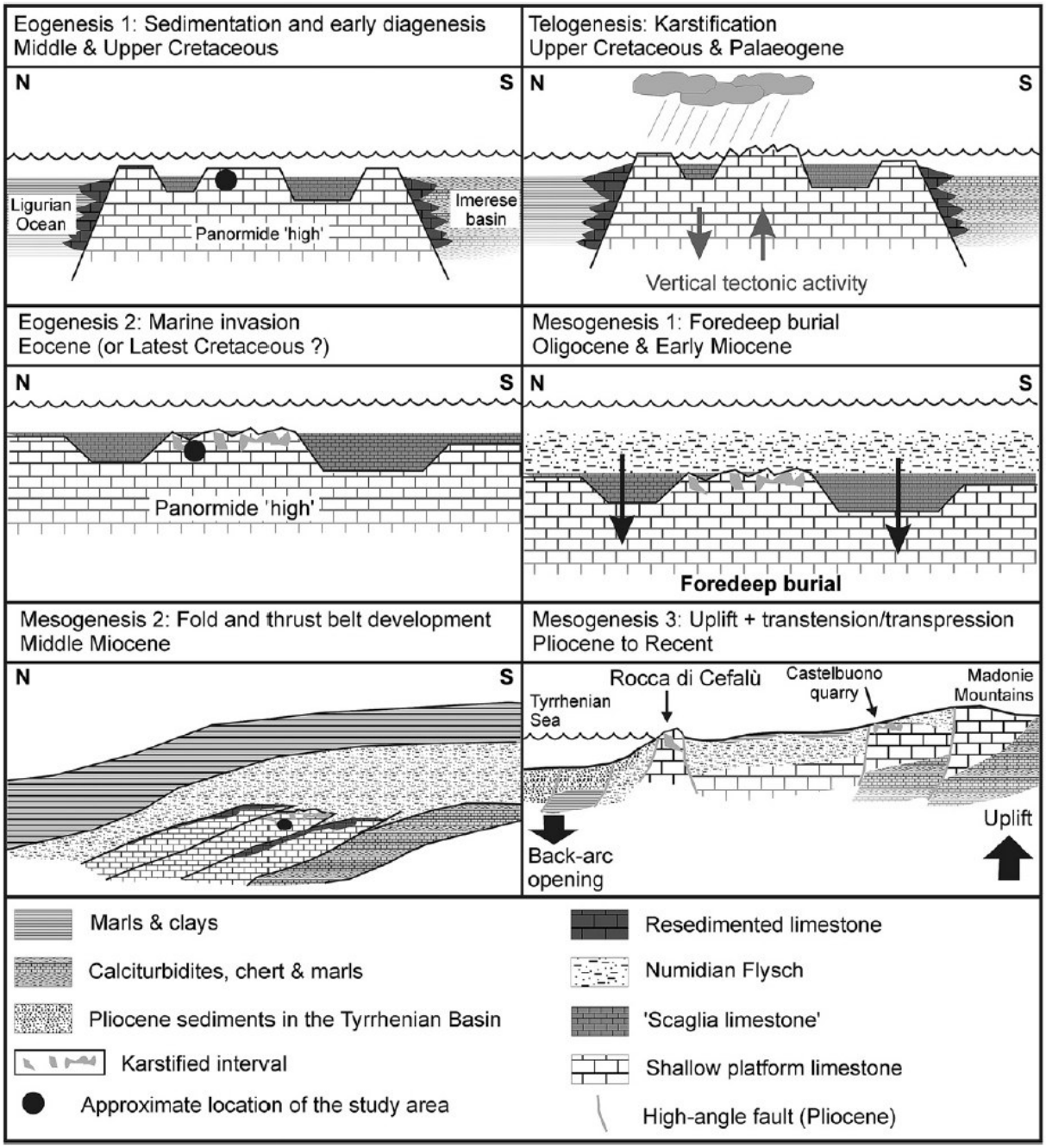


***Fig. 11: schema della storia cinematica e fluidodinamica delle unità cretacee della Piattaforma panormide nella Sicilia centro-settentrionale dal Cretaceo ad oggi***

La presenza di un potenziale serbatoio sotto la grande discordanza regionale tra i calcari cretacei e i sedimenti di avanfossa del *Flysch Numidico* non sarebbe peraltro il solo esempio riscontrato sinora in Italia. Un giacimento offshore nell'avanfossa adriatica si trova anch'esso nei calcari cretacei carsificati appena sotto una grande discordanza regionale tra gli stessi calcari di piattaforma del Cretaceo superiore e i depositi flyschoidi di avanfossa (*Andre e Doulcet*, 1987; *Soudet et al*., 1994).

## 5. CONCLUSIONI

Il contesto geologico dell'ambito territoriale in seno al quale è prevista la realizzazione del tracciato ferroviario Cefalù Ogliastrillo–Castelbuono è rappresentato dunque, quasi esclusivamente, dalla formazione oligo-miocenica del *Flysch Numidico*, al cui interno è stata accertata la presenza di concentrazioni variabili di idrocarburi pesanti C >12, che coinvolgono indistintamente tutte le litofacies di cui esso è composto (argilliti, argille variamente sabbiose, quarzareniti, argille ghiaiose, ecc.).

Tale ambito include anche i due siti di destinazione finale individuati e fatti oggetto anch'essi di apposite indagini.

È stato accertato che la presenza di idrocarburi pesanti nelle concentrazioni rilevate hanno un'origine naturale ed è stato esposto come tale origine possa essere connessa ad aspetti diagenetici, a loro volta legati all'ambiente povero di ossigeno di deposizione dei depositi torbiditici, o, secondo la tesi avanzata da altri autori, a fenomeni di migrazione degli stessi idrocarburi dai sottostanti calcari cretacei a causa della loro compressione avvenuta nel Miocene e favorita ulteriormente dal successivo sistema di faglie plioceniche.

Nel primo caso si tratterebbe di condizioni analoghe a quelle individuate all'interno delle Linee guida predisposte da ISPRA sui Valori di Fondo Naturale (Delibera del Consiglio SNPA. Seduta del 14.11.2017. Doc. n. 20/17), che, seppure siano riferite ad un contesto di terreni "torbosi", appaiono assolutamente applicabili anche alla situazione riscontrata: "*Valori elevati di idrocarburi C >12 (fino a 350 mg/kg) sono stati riscontrati nei suoli torbosi o in generale in suoli con concentrazioni di sostanza organica maggiore del 5%, soprattutto in situazioni di sommersione e quindi carenza di ossigeno. Tali condizioni favorirebbero una lenta trasformazione della sostanza organica in composti ad elevata percentuale di C e H che, all'analisi con metodo ufficiale degli idrocarburi C >12, vengono riconosciuti come tali pur non essendo di origine fossile/petrolifera*" (cfr. nota n. 11 del par. 2.2 "Criticità semantiche ed operative").

Invece nel caso della migrazione degli idrocarburi per compressione dei sottostanti calcari si tratterebbe di un'origine connessa alla tettonica regionale, come illustrato al paragrafo precedente.

A parere dello scrivente non può escludersi che la presenza degli idrocarburi in seno alla formazione del *Flysch Numidico* sia ricollegabile ad entrambe le situazioni, ossia che la loro origine sia connessa sia alle modalità diagenetiche della formazione, sia alle compressioni tettoniche che hanno iniziato a svilupparsi mentre la diagenesi era ancora in corso.

Ad ogni modo è evidente, proprio per le considerazioni geologiche svolte, che l'ambito territoriale con fondo naturale, inteso come "*porzione del territorio geograficamente individuabile in cui può essere dimostrato che un valore di concentrazione di una o più sostanze nel suolo, superiore alle concentrazione soglia di contaminazione di cui alle colonne A e B, Tabella 1, Allegato 5 al Titolo V della parte IV del decreto legislativo 23 aprile 2006, n. 152 sia ascrivibile a fenomeni naturali legati alla specifica pedogenesi del territorio stesso, alle sue caratteristiche litologiche e alle condizioni chimico fisiche presenti*", debba essere riferito alla vasta area di affioramento dell'unità appartenente alla formazione del *Flysch Numidico* denominata *Membro di Geraci Siculo*.

Essa rappresenta una parte del più ampio bacino di sedimentazione dello stesso *Flysch Numidico*, che all'intero comprensorio interessato comprende il sito di produzione e quelli di destinazione dei materiali di scavo.

Pur non entrando nel merito dell'attribuzione del valore di fondo naturale per gli idrocarburi pesanti C > 12 alla formazione geologica indicata, si ritiene che esso debba comprendere la variabilità di tutti i valori misurati, non avendo rilevato né settori di maggiore o minore concentrazione, né facies litologiche caratterizzate da maggiori o minori concentrazioni

Palermo, 14 giugno 2021

**Gian Vito Graziano**
*geologo*

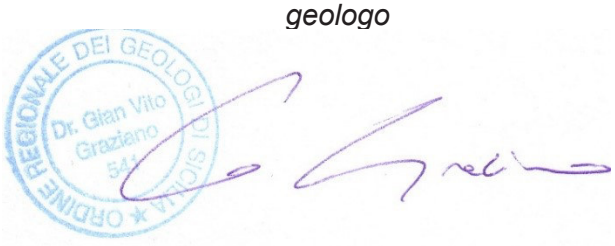

# Appendice

**B. Dewever, I. Berwouts, R. Swennen, L. Breesch e R.M. Ellam**
*Fluid flow reconstruction in karstified Panormide platform limestones (north-central Sicily): Implications for hydrocarbon prospectivity in the Sicilian fold and thrust belt*

Pubblicato su *Marine and Petroleum Geology 27 (2010) 939–958*

Marine and Petroleum Geology 27 (2010) 939–958

Contents lists available at ScienceDirect

Marine and Petroleum Geology

journal homepage: www.elsevier.com/locate/marpetgeo

# Fluid flow reconstruction in karstified Panormide platform limestones (north-central Sicily): Implications for hydrocarbon prospectivity in the Sicilian fold and thrust belt

B. Dewever [a,*], I. Berwouts [a], R. Swennen [a], L. Breesch [b], R.M. Ellam [c]

[a] Katholieke Universiteit Leuven, Aard- en Omgevingswetenschappen, Afdeling Geologie, Celestijnenlaan 200E, B-3001 Heverlee, Belgium
[b] Cretaceous Carbonate Research Centre, University of Copenhagen, Øster Voldgade 10, 1263 København K, Denmark
[c] Scottish Environmental Research Centre (SUERC), Rankine Avenue, Scottish Enterprise Technology Park, East Kilbride G75 0QF, UK

ARTICLE INFO

*Article history:*
Received 20 September 2008
Received in revised form
29 September 2009
Accepted 1 October 2009
Available online 6 December 2009

*Keywords:*
Fluid flow
Oil migration
Karst
Stable isotopes
Microthermometry
Sicily

ABSTRACT

Diagenetic analysis based on field and petrographic observations, isotope and microthermometric data was used to reconstruct the fluid flow history of the Cretaceous shallow water limestones from the Panormide platform exposed in north-central Sicily. Analysis focused on diagenetic products in cavities and dissolution enlarged fractures of the karstified limestones that occur just below a regional unconformity. The fluid flow history could be broken down into five stages that were linked to the kinematic and burial history of the region. (1) Petrography (zoned cathodoluminescence and speleothem textures) and stable isotopes ($6.5 < \delta^{18}O_{V\text{-}PDB} < -3.5‰$ and $0 < \delta^{13}C_{V\text{-}PDB} < -14‰$) indicate that the earliest calcite phase was associated with karstification during emergence of the platform. Limestone dissolution at this stage is important with regard to possible reservoir creation in the Panormide palaeogeographic domain. (2) Fine-grained micrite sedimentation, dated as latest Cretaceous by nannopalaeontology and its $^{87}Sr/^{86}Sr$ isotope ratio (0.7078), marks replacement by marine fluids during subsequent submergence of the karstified platform. (3) The following calcite cement was still precipitated by marine-derived fluids ($-7.0 < \delta^{18}O_{V\text{-}PDB} < -5.0‰$ and $-3.0 < \delta^{13}C_{V\text{-}PDB} < 0.5‰$/$T_m = -2$ to $-5$ °C), but at increasingly higher temperatures ($T_h = 60$–$120$ °C). This has been interpreted as precipitation during Oligocene foredeep burial. (4) Hot ($T_h = 130$–$180$ °C), low saline ($T_m < -2.5$ °C) fluids with increasingly higher calculated $\delta^{18}O_{SMOW}$ signatures (+6 to +14‰) subsequently invaded the karst system. These fluids most likely migrated during fold and thrust belt development. The low salinity and relatively high $\delta^{18}O_{SMOW}$ signatures of the fluids are interpreted to be the result of clay dewatering reactions. The presence of bitumen and associated fluorite with hydrocarbon inclusions at this stage in the paragenesis constrains the timing of oil migration in the region. (5) Finally, high saline fluids with elevated $^{87}Sr/^{86}Sr$ (0.7095–0.7105) signatures invaded the karst system. This last fluid flow event was possibly coeval with localized dolomitization and calcite cementation along high-angle faults of Pliocene age, as suggested by identical radiogenic signatures of these diagenetic products.



## 1. Introduction

Due to the decline in hydrocarbon reserves in classical sedimentary basins (e.g. the North Sea), exploration nowadays also focuses on areas with higher exploration risks such as fold and thrust belts (FTB's) (e.g. Crane, 1990; Mascle et al., 1996). The exploration risks in FTB's amongst others include the structural complexity of the subsurface and the diagenetic history (Oliver, 1986; Bradbury and Woodwell, 1987). The diagenesis, which has ample implications for the porosity and permeability in reservoirs, especially in limestones, typically involves both early diagenetic modifications and late syn-deformational fluid flow events (e.g. Van Geet et al., 2002).

A number of numerical fluid flow reconstruction studies have been performed in different FTB's worldwide (e.g. Machel and Cavell, 1999; Moretti et al., 2002; Schneider, 2003; Swennen et al., 2004; Roure et al., 2005; Vandeginste et al., 2005). These studies used an integrated structural-diagenetic approach to decrease the risks associated with hydrocarbon exploration in the tectonically

* Corresponding author at: Maersk Oil & Gas, Esplanaden 50, 1263 København K, Denmark. Tel.: +45 2748 3531.
*E-mail addresses:* ben.dewever@gmail.com (B. Dewever), isaac.berwouts@ees.kuleuven.be (I. Berwouts), rudy.swennen@ees.kuleuven.be (R. Swennen), lb@geo.ku.dk (L. Breesch), r.ellam@suerc.gla.ac.uk (R.M. Ellam).

0264-8172/$ – see front matter © 2009 Elsevier Ltd. All rights reserved.
doi:10.1016/j.marpetgeo.2009.10.018

complex areas. The fluid flow reconstruction studies mainly focused on diagenetic products in structural elements such as faults, veins and stylolites. Their crosscutting relations and structural orientations are used to constrain respectively the relative and absolute timing of different fluid flow events (Travé et al., 1998; Travé and Calvet, 2001; Ferket et al., 2004; Breesch et al., 2007). In addition, the origin of the fluids and the physico-chemical conditions of fluid flow were deduced using geochemical and microthermometric techniques.

Highly permeable paleokarst intervals are often locations of major fluid flow (e.g. Benchilla et al., 2003; Boni, 1986; Min and Wu, 1998; Valenza et al., 2000; Mabhoubi et al., 2002; Amthor and Friedman, 1992). However, these reservoir systems have the disadvantage that it is more difficult to constrain the absolute timing of the many diagenetic events typically seen in paleokarst reservoirs, relative to the timing of a few diagenetic phases associated with a geochronologically well-constrained structural event. In this paper, we demonstrate how the rational use of field relationships and geochemical and microthermometric tools allows us to link the relative timing of diagenetic and fluid flow events in a paleokarst system to the absolute time scale, burial history and kinematic evolution. Note that the primary aim of the study was to reconstruct fluid flow through time, not to characterize the reservoir or to reconstruct the porosity history as other authors have done with karstified limestones (e.g. Kerans, 1988; Wagner, 1990; Bourque et al., 2001).

The presence of bitumen attests to past hydrocarbon migration and/or storage in the karst reservoir. The results of the fluid flow reconstruction allow for the first time to constrain the timing of oil migration in the region to a certain extent. Similar plays in the Mediterranean region indicate the importance of Cretaceous karstification for reservoir development in the region (e.g. Andre and Doulcet, 1987; Soudet et al., 1994).

## 2. Geological background

### 2.1. Sicily

Sicily is located in the western Mediterranean and the island's landscape is dominated by the Sicilian FTB, which is part of the Maghrebides (Fig. 1). The Sicilian FTB belongs to a group of FTB's that encircle most of the western Mediterranean Sea; i.e. the western Alps and the Apennines in France and Italy, the Maghrebides in Sicily and northern Africa and the Betic Cordillera in Spain (Rosenbaum and Lister, 2004a) (Fig. 1A). The deformation that was responsible for structuring these FTB's started in the Oligocene and continues until today (Rosenbaum and Lister, 2004a). It is the result of the convergence of the African and European plates and the northward subduction of the Ligurian Ocean, a small oceanic domain that occurred in between both continents (Elter et al., 2003; Rosenbaum et al., 2002; Rosenbaum and Lister, 2004b).

Sicily is composed of an undeformed foreland in the south with a foredeep located just north of the foreland (Fig. 1B). The northern part of the island consists of an imbricate thrust stack in which three important tectonic units can be recognized. From top to bottom in the structural edifice these are: (1) the Peloritani units; (2) the Sicilide units; and (3) the Internal units (Bello et al., 2000; Catalano et al., 1996, 2000; Elter et al., 2003) (Fig. 1B).

The Peloritani units consist of Mesozoic and Tertiary sediments underlain by a metamorphosed basement and European continental crust. The Sicilide units are made up by deformed Jurassic to Eocene clays and marls which formed the sediment cover of the subducted Ligurian Ocean. The Internal units (Fig. 1B) consist of deformed Mesozoic and Tertiary sediments that are underlain by thinned African continental crust (Elter et al., 2003). The Internal sediments were deposited in different palaeogeographic domains (the Panormide, Saccense, Imerese, Sicani, Trapanese and Hyblean domains) (Catalano et al., 1996). The latter palaeogeographic domains were differentiated during Jurassic transtension and opening of the Tethys Ocean when a basin and range topography was established on the African passive margin (Catalano et al., 1996; Stampfli and Borel, 2002).

Compressive deformation in Sicily started in the Late Oligocene and its peak is dated as Middle Miocene (Roure et al., 1990; Catalano et al., 1996; Bello et al., 2000). Deformation resulted in a thin-skinned FTB with several décollement levels. In-sequence thrusting with southward displacement of the thrust front was often followed by the accretion of tectonically deeper levels (Bello et al., 2000; Granath and Casero, 2004; Nigro and Renda, 2000). In the northern part of the island, the tectonic edifice is strongly modified by the development of a complex pattern of EW, NS, NW–SE and NE–SW oriented normal and strike-slip faults (Ghisetti and Vezzani, 1984; Giunta et al., 2000a). The faults are Pliocene to recent in age and are the result of the opening of the Tyrrhenian Sea as a back-arc basin (Jolivet and Faccenna, 2000).

### 2.2. Panormide platform

#### 2.2.1. Palaeogeography and sedimentology

The Cretaceous platform carbonate rocks that are the subject of the present study are located in north-central Sicily, in the Madonie Mountains (Fig. 1B,C). The limestones were deposited in the Panormide palaeogeographic domain (Lentini and Vezzani, 1974). The Panormide is the only palaeogeographic domain on the African passive margin that was characterized by shallow platform sedimentation during the Cretaceous. It was bounded to the south by the Imerese basin and to the north by the Ligurian Ocean.

During the Cretaceous, the Panormide 'high' was characterized by a complex facies distribution (Miuccio et al., 2000). This is exemplified by the existence of contemporaneous shallow rudist-dominated carbonates (Di Stefano and Ruberti, 2000) and pelagic micritic limestone deposits, referred to as 'scaglia' in Sicily (Catalano et al., 1973), relatively close to each other. The presence of these different facies was controlled by the antecedent topography that resulted from Jurassic extensional tectonic activity during opening of the Neotethys (Nigro and Renda, 2002; Di Stefano et al., 2002). In the study area, the Panormide Cretaceous rocks are underlain by a thick series of Triassic and Jurassic platform limestone that are partially dolomitized. An important regional unconformity with associated palaeorelief separates Cretaceous limestones from overlying Numidian flysch sediments that are 2–3 km thick (Figs. 1C and 2). The Numidian flysch represents the sedimentation during foredeep development and consists of shales and coarse sandstone bodies (Johansson et al., 1998).

#### 2.2.2. Burial and kinematic history

A burial history for the region is not available from the literature. Using stratigraphic thicknesses described by Brocquet (1970) and Lentini and Vezzani (1974) and general field observations, a tentative burial curve was constructed (Fig. 3). The time line also reflects the different stages in the kinematic history of the region. The curve should be used with care since it is not supported by any temperature data or by maturity data such as vitrinite reflectance. Furthermore, compaction was not taken into account either. A burial envelope was used to mark reasonable estimated minimum and maximum burial depths through time. A geothermal gradient of 30 °C/km was used to link temperature to depth. Note that the geothermal gradient is only a rough estimate and most likely fluctuated through time, especially during FTB development.

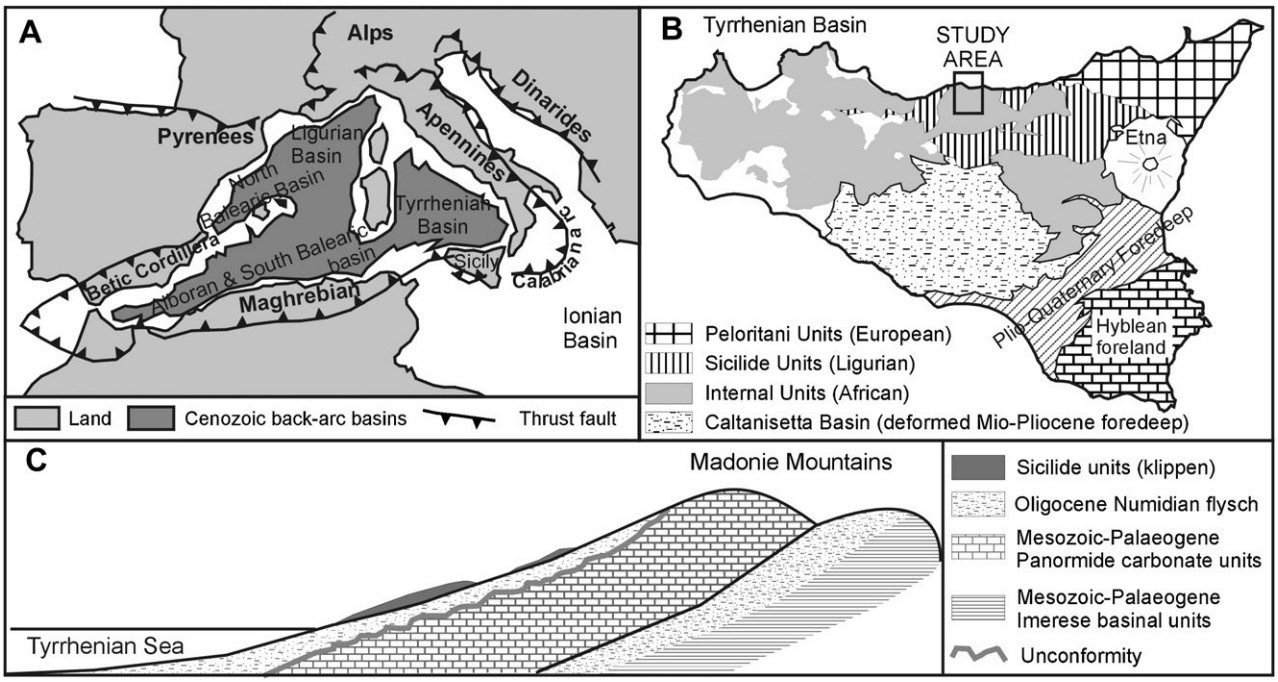


**Fig. 1.** (A) Geological setting in the western Mediterranean area with an arcuate-shaped mountain chain that encircles Cenozoic back-arc basins. (B) Simplified structural map of Sicily showing the main components of the Sicilian fold and thrust belt and the location of the study area (rectangle). (C) Simplified N–S oriented cross-section through the study area that shows the structural edifice after Miocene compressive deformation. The cross-section illustrates stratigraphic relations in the study area. The sketch omits later normal and strike-slip fault activity during Pliocene to Recent transtension/transpression.

The burial curve starts in the Late Cretaceous, which reflects the general age of the sediments just below the unconformity (Lentini and Vezzani, 1974). The presence of a paleo-relief and the unconformity between Late Cretaceous and Late Oligocene sediments indicates long-standing emergence and erosion during this period of time (Fig. 2). It is not possible to assess the amount of limestone that has been chemically and physically weathered. Weathering rates are dependant on the climate, the uplift rates, the limestone rock type etc. In Fig. 3, a couple of hundred metres of burial in the Cretaceous have been accepted.

At places, patches of Late Cretaceous to Eocene pelagic mudstone sediment (so-called 'scaglia') drape palaeo-topographic depressions on the Cretaceous limestone unconformity. The sediments are typically deposited in relatively deep-water conditions (couple of hundred metres). The patchy sediment distribution and

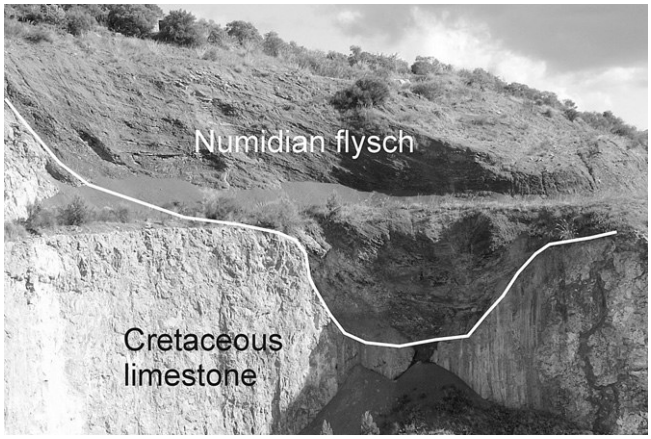


**Fig. 2.** Field photograph showing the unconformity between the Cretaceous karstified limestone and the Oligocene Numidian flysch in the abandoned quarry at Castelbuono. Palaeorelief is illustrated by the white line, which demarks the top of the limestone.

the nature of the sediment could be interpreted in a number of ways: (1) there were several short periods of sedimentation alternating with periods of erosion and karstification during submergence; or (2) there was only one phase of emergence, followed by deep-water conditions where non-deposition and/or erosion occurred. In any case, submergence and emergence were most likely controlled by vertical tectonic activity. The latter was induced by Alpine compression in the south (Nigro and Renda, 2002). Main argument for the presence of such tectonic activity in the region is the existence of thick breccia units that are Late Cretaceous and Palaeogene in age (Di Stefano et al., 1996). They are closely related to major fault zones that delimit palaeogeographical entities.

Accurate evaluation of the overthrusted sediment thickness is impossible since the sediments from the Sicilide unit are partially to completely eroded. Thickness was certainly over 500 m (Broc-quet, 1970; Lentini and Vezzani, 1974) but could have been up to 3 km according to Aldega et al. (2007). Burial history reconstruction becomes even more tentative during thrusting of the Panormide unit over the Imerese unit. It is not clear if thrust movement was associated with uplift (dashed line in Fig. 3) or additional burial (full line in Fig. 3). A simplified sketch of the tectonic edifice in the study area is shown in Fig. 1C. The Sicilide units were thrusted over the Panormide units in Burdigalian times (Nigro and Renda, 2000). At present, these units are only exposed in tectonic klippen, due to uplift and erosion that has taken place since the Pliocene. The Panormide units in turn have overthrusted the Imerese units in the Tortonian (Nigro and Renda, 2000). These units consist of Imerese Oligocene flysch and Mesozoic 'scaglia', basinal calciturbidites, cherty limestones and pelagic marls (Fig. 1C) (Lentini and Vezzani, 1974).

Onset of uplift in the region was very late. The presence of Pliocene marine Trubi deposits above 2000 m altitude in the Madonie Mountains, located just south of the study area, implies an uplift of about 0.55 mm/year since the Middle Pliocene. The start of extensional tectonic activity is somewhat debated but must have

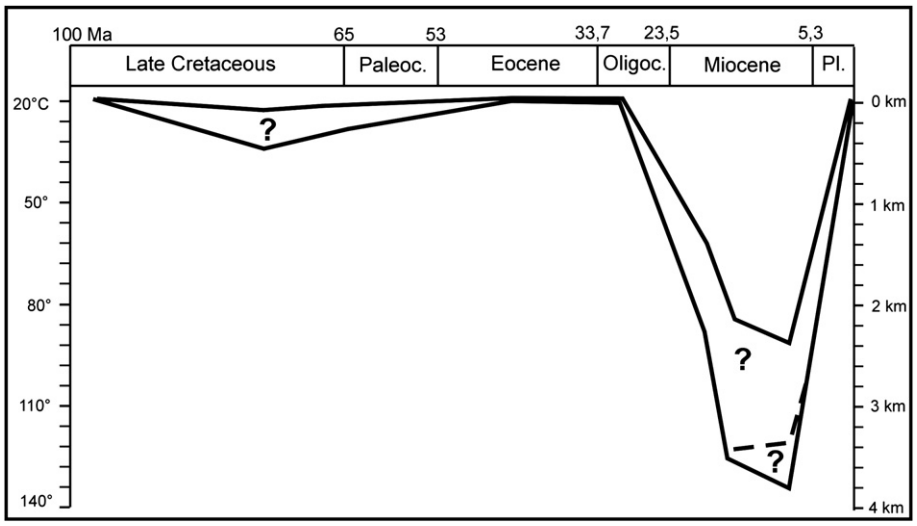


**Fig. 3.** Tentative burial curve envelope showing estimated maximum and minimum burial depth for the Cretaceous karstified limestones, based on stratigraphic information and general geological background.

occurred between the latest Middle Miocene when compressional activity ceased in the region and the Middle Pliocene when uplift was initiated. The original compressional tectonic edifice in the study area is largely overprinted by extensive normal and strike-slip faulting associated with uplift and opening of the Tyrrhenian Sea.

## 3. Methodology

The paragenetic sequence of diagenetic events was deduced from field and petrographic observations. Geochemical and microthermometric characteristics of consecutive diagenetic products then allowed to subdivide the paragenesis or fluid flow history into five different stages. Finally, it was possible to link the paragenesis to the kinematic and burial history. This was achieved by using the fluid flow history (e.g. influx of meteoric or marine fluids, low or high salinity, high or low temperature fluids, etc.). However, also palaeontology (nannofossil), geochemistry ($^{87}Sr/^{86}Sr$) and structural geology were involved in this process.

Diagenetic products (calcite and dolomite) were sampled in cavities and dissolution enlarged fractures and along Pliocene high-angle faults in Cretaceous platform limestones. The samples were cut, polished, etched and stained with Alizarin-red-S and potassium ferricyanide (Dickson, 1966). Petrographic observations were carried out using standard petrographic microsocopy and fluorescence microscopy. An in-house built device was used for cathodoluminescence observations (150–250 μA beam current and 12–14 kV gun potential).

Carbonate powders for carbon and oxygen stable isotope and $^{87}Sr/^{86}Sr$ isotope analysis were drilled with a dental microdrill. For stable isotope analysis, carbonate powders were reacted with 100% phosphoric acid (density >1.9 g cm$^{-3}$, Wachter and Hayes, 1985) at 75 °C in a carbonate preparation line (Carbo-Kiel – single sample bath) connected to a Finnigan Mat 252 mass spectrometer. All values are reported in per mil (‰) relative to Vienna Pee Dee Belemnite (V-PDB). Reproducibility was checked by replicate analysis of laboratory standards and was better than ±0.01‰ for $\delta^{13}C$ (1σ) and ±0.03 ‰ for $\delta^{18}O$ (1σ). The oxygen values for dolomite were corrected using the fractionation factors of Rosenbaum and Sheppard (1986).

For $^{87}Sr/^{86}Sr$ isotope analyses, calcite samples were leached in $NH_4CH_3COOH$ 1 N prior to acid digestion in 2.5 M HCl. Sr was separated using Bio-Rad AG50W X8 200–400 mesh cation exchange resin. Sr samples were loaded onto single Ta filaments with 1 N of phosphoric acid and analysed on a VG Sector 54–30 multiple collector mass spectrometer, operated in the peak-jumping mode with data collected as 15 blocks of 10 ratios. A $^{88}Sr$ intensity of 1 V ($1 \times 10^{-11}$ A) ± 10% was maintained. Data were corrected for mass fractionation using $^{86}Sr/^{88}Sr = 0.1194$ and an exponential law. NIST SRM987 gave 0.710258 ± 11 (1σ, $n = 16$) during the course of this study.

Microthermometric analysis of fluid inclusions was carried out on double polished wafers. Petrographic observations allowed differentiating primary from (pseudo)-secondary inclusions (Goldstein and Reynolds, 1994). The presence of hydrocarbon inclusions was evaluated by using fluorescence microscopy. A Linkam heating–cooling stage was used for microthermometric analysis. Calibration was performed by measuring phase changes in synthetic standard fluid inclusions. Reproducibility of final melting temperature of ice ($T_m$) was within 0.2 °C and of homogenization temperature ($T_h$) within 2 °C. All inclusions in a piece of wafer were first cooled to −120 °C and then slowly heated in order to measure $T_{mi}$ and $T_e$ (if observable) and $T_m$. Hereafter, the inclusions were slowly heated in order to obtain $T_h$. No pressure corrections have been made.

## 4. Field and petrographic observations

Two locations that lie about 15 km apart from each other were studied: a rocky coastline just north of the Rocca di Cefalù (location: 38°02′26″ & 14°01′40″ E) and an abandoned limestone quarry in Castelbuono (location 37°58′17″ N & 14°06′23″ E). According to the geological map of the study area (Lentini and Vezzani, 1974), the studied outcrops at the Rocca di Cefalù belong to the Upper Cretaceous Calcari di Cefalù Formation while the outcrops in the Castelbuono quarry are part of the Lower Cretaceous Calcari di Pizzo di Canna Formation. Both outcrops thus represent different stratigraphic ages and are also characterized by different sedimentology. The outcrops in Cefalù are dominated by rudist grainstones with intercalated wacke- and mudstones. In Castelbuono, bioclasts are largely absent and the studied stratigraphic interval is dominated by mudstones with intercalated rudist pack- to wackestones. Both outcrops have in common that an important karst system developed in the Cretaceous limestones.

The karst system is best developed just below the regional unconformity between Cretaceous limestones and Oligocene Numidian flysch. The unconformity level in the Castelbuono quarry clearly shows the existence of palaeorelief (Fig. 2), suggesting an important period of emergence and erosion between the Late Cretaceous and the Oligocene. Furthermore high-angle faults of Pliocene age have been encountered in both outcrops (Giunta et al., 2000a).

In the following sections, the diagenetic products that occur in the karst system and in the high-angle faults are described. Each diagenetic product is given a double letter code and a number (e.g. K-Dol-1), corresponding to the place where it occurs (karst = K & fault = F), the type of diagenetic mineral (dolomite = Dol; calcite = Cal; fluorite = Fl; sedimentary infill = Sed) and its position in the paragenesis.

### 4.1. Karst system

The karst system consists of a complex network of cavities with a maximum width of ±30 cm that are interconnected by dissolution enlarged fractures of few millimetres to a couple of centimetres wide. Many of these fractures and cavities have been partially to completely filled by different diagenetic phases. The sketch in Fig. 4 shows these diagenetic phases and the macroscopic overgrowth relationships. Based on the latter, a chronological presentation of their macroscopic and microscopic features follows below. A more profound paragenesis will be worked out later in the text (see interpretation).

#### 4.1.1. K-Cal-1

The first cement that lines karst cavities and related dissolution enlarged fractures consists of calcite cement crusts. Macroscopically, the cement is characterized by a banded pattern with different shades of grey (Fig. 5A). The calcite is characterized by a columnar to elongate blocky texture with abundant solid inclusions. In between layers of parallel columnar crystals, clusters of scalenohedral calcite crystals occur (Fig. 5B). The calcite exhibits alternating non-, dull and bright luminescent zones. The original sharp luminescence boundaries between different zones have often been obliterated by a patchy dull orange to brown luminescence pattern (Fig. 4C). This early cement is volumetrically the most important phase in the karst system.

#### 4.1.2. K-Sed-1 & K-Cal-2

After the precipitation of K-Cal-1, remaining karst cavities were partially or completely filled by white to grey sediment consisting of micrite. Small changes in grain size are responsible for observed layered patterns of this sedimentary infill (Fig. 5G). Some carbonate grains are broken parts of foraminifer skeletons. Nannofossil assemblages from two micrite samples indicate a Late Campanian age for the sediment analysed (pers. comm. C. Müller). The micrite is further characterized by dull to bright orange cathodoluminescence. Locally, minor columnar and non-luminescent K-Cal-2 cement was precipitated before K-Sed-1.

#### 4.1.3. K-Cal-3, K-Dol-1 & K-Cal-4

K-Cal-3 is an elongate to equant Fe-poor calcite cement that covers K-Sed-1 and/or K-Cal-1 (Fig. 5G). The cathodoluminescence of K-Cal-3 varies from non- over bright to dull luminescent. Occasionally, the Fe-poor rhombohedral dolomite cement with crystal growth zones, K-Dol-1 (Fig. 5D,H) overgrows K-Cal-3. The core of the dolomite crystals is non-luminescent whereas the outermost part of the crystals is characterized by red luminescence. Other cavities are partially filled with white to brown coloured Fe-poor K-Cal-4 calcite cement (Fig. 5E,F). This calcite is characterized by uniform dull brown luminescence. The cement consists of large equant crystals with abundant mechanical calcite twinning.

#### 4.1.4. K-Cal-5

K-Cal-5 covers K-Cal-3 and K-Cal-4 cements in the karst cavities and also occurs in fractures that crosscut K-Cal-4 (Fig. 4). This phase is the oldest ferroan phase in the karst system, as revealed by staining. The crystals are further characterized by a uniform dull brown luminescence and an equant texture. Some K-Cal-5 crystals

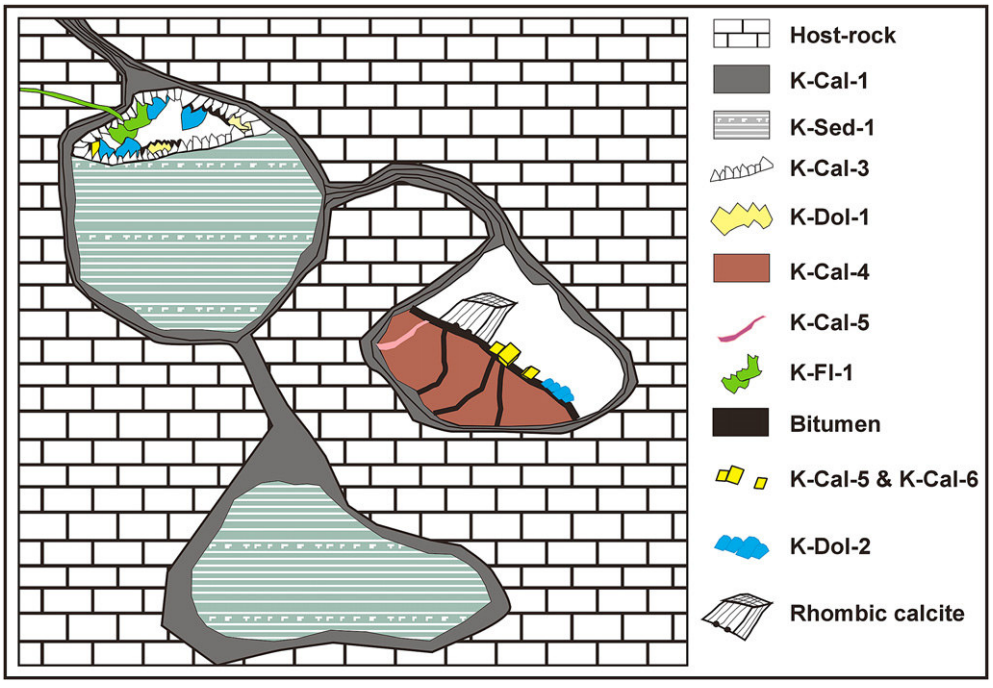


**Fig. 4.** Simplified sketch of the different diagenetic products and their time relationships in the karst network.

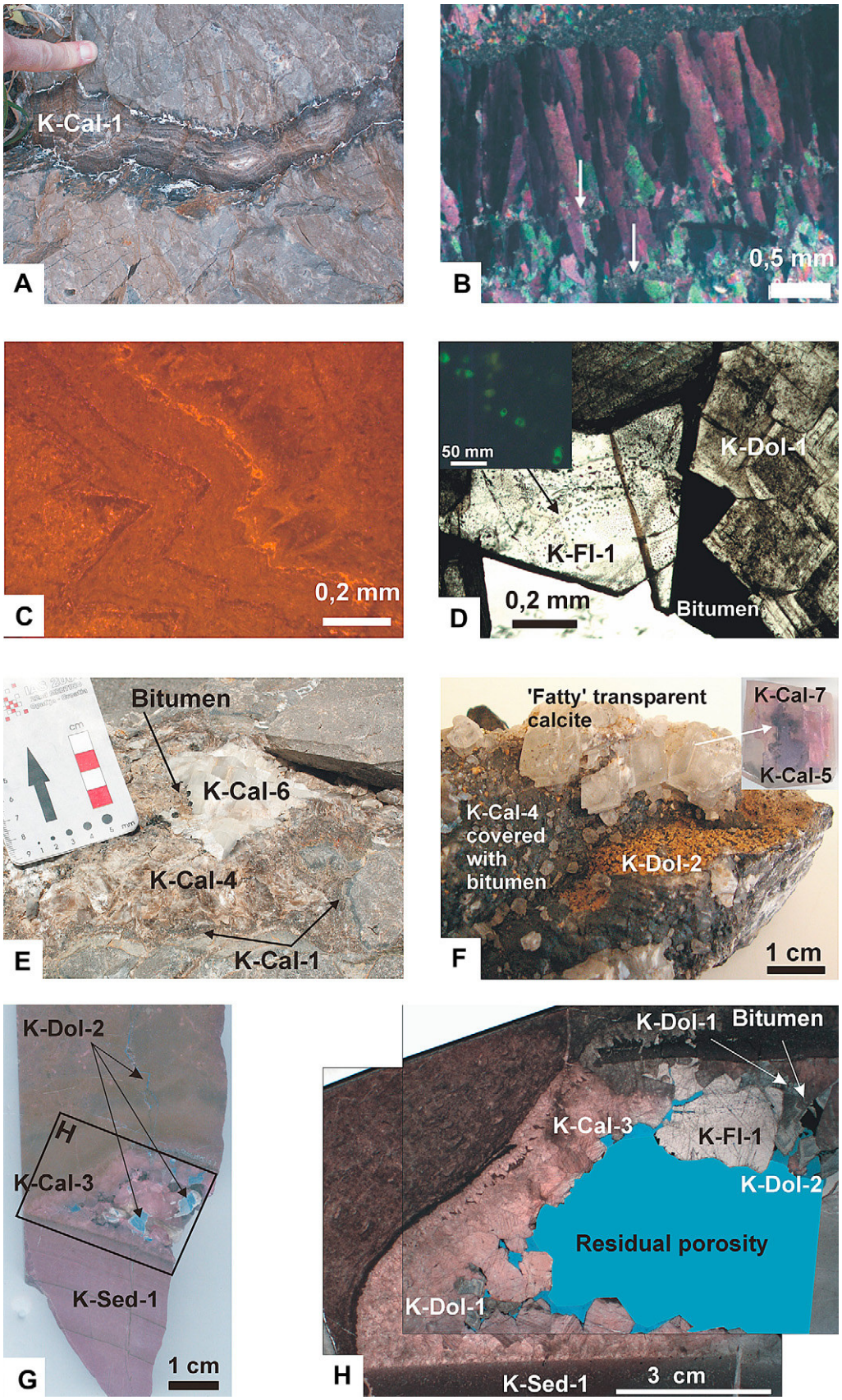


**Fig. 5.** (Micro)-photographs showing the different diagenetic products from within the karst network. (A) K-Cal-1 cement in a dissolution enlarged fracture. The texture is defined by cement bands that are characterized by different shades of grey. (B) Alternating zone of elongate blocky and scalenohedral calcite crystals in K-Cal-1. (C) Zoned luminescence pattern in K-Cal-1 that is partly obliterated by patchy and blotchy patterns, representing recrystallization. (D) K-Fl-1 and K-Dol-1 phases with bitumen (black) that covers both

show well-developed rhombic crystal habits that have a lustrous shine and are remarkably translucent (Fig. 5F).

#### 4.1.5. Bitumen & K-Fl-1

The presence of bitumen in the cavities and in small veinlets in the carbonates indicates that oil migrated through the studied rock interval and/or was stored in the Cretaceous limestone karst reservoirs. Bitumen is abundant in many karst cavities, especially in Castelbuono. It covers all the above-mentioned phases but is overgrown by all the later phases (Fig. 5E,F). In one sample, fluorite is intimately associated with the bitumen, being embedded in a large bitumen spot in plane view in a thin section. With the use of fluorescence microscopy, large two-phase hydrocarbon inclusions have been observed in fluorite crystals (Fig. 5D). The inclusions are orange to green fluorescent under UV-light which is indicative for the presence of medium-gravity oils (Burruss, 1991). There are no other diagenetic phases that displayed the presence of fluorescent hydrocarbon inclusions with the use of UV-light.

#### 4.1.6. K-Dol-2 & K-Cal-6

K-Dol-2 & K-Cal-6 directly overgrow bitumen and/or earlier cements. K-Cal-6 undoubtedly postdates K-Dol-2 since it fills remaining porosity between the dolomite crystals. K-Dol-2 possesses curved crystal faces, which is a feature typical for saddle dolomites (Searl, 1989). The crystals stain blue indicating a ferroan composition (Fig. 5G) and the dolomite is non-luminescent. K-Cal-6 is also non-ferroan as shown by staining and has translucent crystals (Fig. 5D). K-Cal-6 often occurs as a late crystal rim overgrowing earlier K-Cal-5 crystals. A thin zone of bitumen often occurs in between both phases (Fig. 5F). At the same time, K-Cal-5 is slightly corroded just below the bitumen cover. K-Cal-6 shows clear and sharp cathodoluminescence zonations varying between bright yellow and dull orange luminescent.

#### 4.1.7. Rhombic calcite

Finally, large white rhombic calcite crystals occur in the karst system. This calcite postdates oil migration since it overgrows bitumen droplets (Fig. 5E) but overgrowth relationships with other diagenetic phases in the karst system are missing. Rhombic calcite is not transparent and staining indicates variation in the iron content. Their cathodoluminescence is dull brown. Abundant thin cleavage twins have developed in these large crystals.

### 4.2. High-angle faults

High-angle faults were recognized in the field by the existence of striated fault scarps (Fig. 6A) associated with a white calcite cemented fault breccia (Fig. 6B). The age of the high-angle faults is Pliocene and the faults result from the opening of the Tyrrhenian Basin in a transtensional/transpressional regime (Del Ben and Guarnieri, 2000; Giunta et al., 2000a). The structural orientation of the faults is highly variable but the main orientations are NS, EW, NNE–SSW and WNW–ESE (Giunta et al., 2000b). Striations indicate both normal and oblique movements along the faults.

Three different breccia types could be recognized in the high-angle fault zones. The breccias are all monomict but have varying macroscopic and microscopic characteristics. They can be classified as follows using the classification of Morrow (1982):

#### 4.2.1. Breccia type 1

Breccia type 1 is most commonly encountered and can be classified as rubble cemented float-breccia (Fig. 6B). The breccia fragments in the fault zone consist of surrounding host-rock limestone that have been partially dolomitized. Fe-poor calcite cement has occluded original porosity between the breccia fragments. In a number of fault zones typified by breccia type 1, there is quartz sand infill mixed with foraminifera, indicating a marine origin of this infill. The sands have been dated as Plio–Pleistocene, based on the macro- and microfauna present (pers. comm. Dr. G. Barrecca), indicating that the fault was connected to the Plio–Pleistocene seafloor surface in some way.

#### 4.2.2. Breccia type 2

Breccia type 2 can be classified as crackle to mosaic cemented pack-breccia. Opposite to the other two breccia types, breccia type 2 is not only restricted to narrow and well defined fault zones but the original host-rock limestone is heavily brecciated over a few to tens of metres in the neighbourhood of the fault zone. The stained rock samples from breccia type 2 are characterized by a stockwork of small veinlets that are filled with Fe-poor dolomite (Fig. 6C).

#### 4.2.3. Breccia type 3

Breccia type 3 classifies as mosaic to rubble cemented float- to pack-breccia. This breccia type only was observed in few locations. Breccia fragments from the original limestone host-rock are completely dolomitized. Original porosity between breccia fragments has been occluded by calcite and/or dolomite cement (Fig. 6D).

A number of different diagenetic phases were recognized in these breccias. Dolomite was encountered in and around fault zones both as cement (Fig. 6C) and as dolomitized patches (Fig. 6D) whereas the limestone host-rock away from fault zones is not dolomitized. Three different types of dolomite are defined based on their occurrence:

#### 4.2.4. F-Dol-1

Dolomitized limestone host-rock fragments that occur as high-angle fault breccia fragments are referred to as F-Dol-1. The original limestone textures may still be recognized. The dolomitized limestone shows evidence of multiple fracturing events. The dolomite is characterized by xenotopic-a to idiotopic-s texture and is Fe-poor (Sibley and Gregg, 1987).

#### 4.2.5. F-Dol-2

F-Dol-2 encompasses the dolomite in the fracture stockwork of breccia type 2. This dolomite is characterized by an idiotopic-e to idiotopic-s texture according to the classification of Sibley and Gregg (1987) and is Fe-poor again (Fig. 6E,F). Dolomite crystals consist of small sub- to euhedral rhombohedra with a turbid core and a more transparent rim. In some cases, the dolomite is brown coloured. The dolomite crystals are zoned under cathodoluminescence with alternating dark red and non-luminescent zones. Macroscopically, the dolomite is aligned along fractures (Fig. 6B). However, microscopic observations suggest that F-Dol-2 did not just fill the open fracture space. This is illustrated in Figs. 6E,F where it is clear that rhombohedral dolomite crystals also

phases. Inclusions of hydrocarbons in the fluorite are visible. They are characterized by green-yellow colours under fluorescence microscopy (see inset). (E) Partially eroded karst cavity with K-Cal-1 occurring at the edges of the cavity. Brown K-Cal-4 cement fills most of the cavity. Rhombic calcite covers bitumen droplets. (F) Sample from within a karst cavity that mainly consists of K-Cal-4, covered with bitumen. K-Dol-2 overgrows and postdates bitumen. Glossy transparent crystals show a thin line of bitumen in between two-phases, Fe-rich crystal core (K-Cal-5 and Fe-poor crystal rim (K-Cal-6). (G) Digital scan from sample with karst cavity. The cavity is partially filled with layered K-Sed-1. The top of the cavity is filled with later diagenetic products that are shown in (H). (H) Microphotograph from the cavity, identifying residual porosity, micritic K-Sed-1, equant K-Cal-3 cement partially replaced by K-Dol-1, K-Fl-1 and K-Dol-2. Some bitumen attests of the emplacement of hydrocarbons.

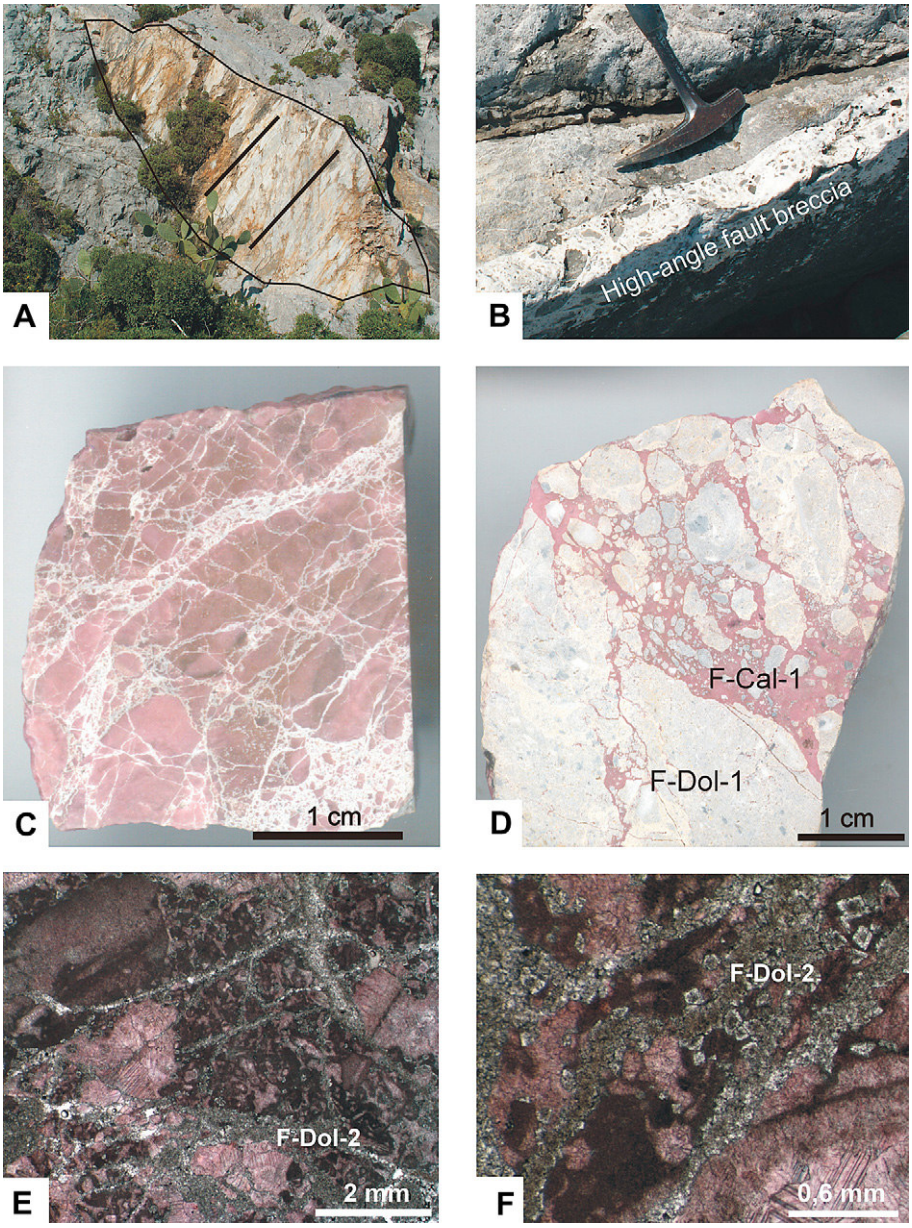


**Fig. 6.** (A, B) Field photographs from high-angle faults in the Cefalù study area. (A) Shows a recent fault scarp where dolomite occurs and (B) illustrates the rubble cemented float-breccia that is frequently encountered in high-angle faults. The white matrix consists of F-Cal-1 and the breccia fragments are composed of host-rock. (C, D) Digital scans from stained hand samples illustrating the different types of fault breccia that were encountered in the high-angle faults. (C) Scan representing the stockwork of breccia type 2 where the fractures contain unstained F-Dol-2 and the red-stained host limestone fragments. (D) Scan of breccia type 3 consisting of a mosaic to rubble cemented float- to pack-breccia with angular to sub-rounded fragments of the host-rock that have been dolomitized (F-Dol-1). The matrix consists of F-Cal-1. (E, F) Microphotographs from stained thin section illustrating the dolomite texture in F-Dol-2 where rhombic crystals fill up the fracture space in breccia type 2.

partially replace the original limestone host-rock around well defined fracture traces.

#### 4.2.6. F-Dol-3 & F-Cal-1

F-Dol-3 refers to all Fe-poor dolomite cements that occur in veins and in fault breccias. This phase is characterized by well-developed rhombohedral crystals with growth zones and a planar-e texture.

Finally, F-Cal-1 is abundantly present in the matrix of the different breccia types introduced above. F-Cal-1 typically consists of Fe-poor calcite cement and postdates all the above-mentioned dolomite phases. It is characterized by an equant crystal texture and presence of abundant solid inclusions in the crystals. The calcite is very dark to non-luminescent with some very bright yellow luminescent zones. The cement shows no twinning or cleavage development. This suggests that crystals have not been affected by major burial or tectonic stresses.

Faults are much more common in the Cefalù outcrop where they display all the above-mentioned characteristics. In the quarry in Castelbuono, only two smaller faults were observed with F-Cal-1 the only cement present in these faults.

## 5. Geochemistry

### 5.1. Oxygen and carbon stable isotope results

Stable isotope analysis was performed on the different carbonate diagenetic phases encountered in Cefalù and Castelbuono (Fig. 7).

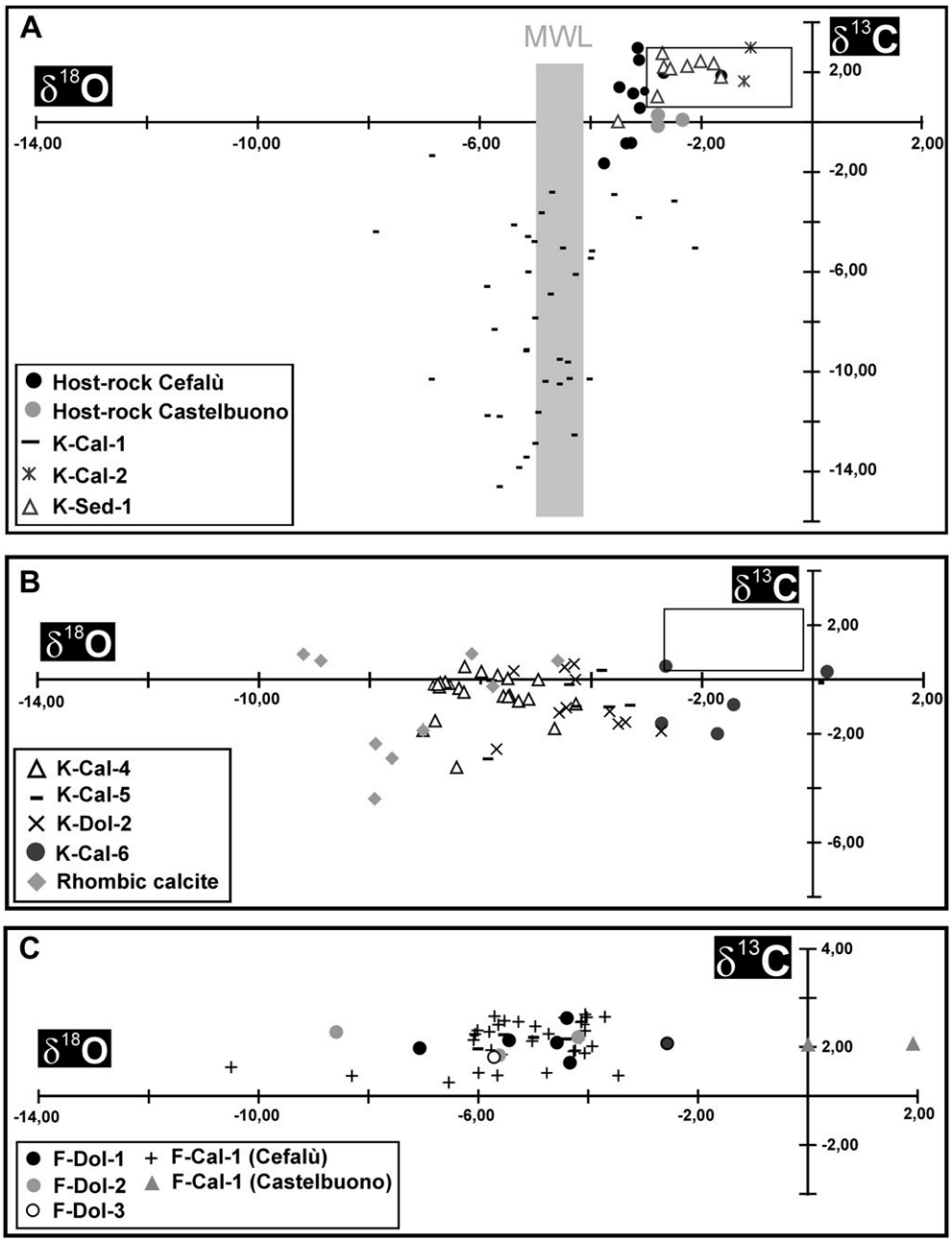


**Fig. 7.** $\delta^{18}O$–$\delta^{13}C$ cross-plots showing the stable isotope results for (A) the host-rock and earliest diagenetic phases in the karst network (K-Cal-1 and K-Sed-1), (B) diagenetic phases in the karst network that postdate K-Sed-1 and (C) diagenetic products from the high-angle faults. The meteoric water line (MWL) was estimated for the Late Cretaceous, based on the palaeogeographic latitudinal position of the Panormide at that time (20°NB; Stampfli and Borel, 2002), $\delta^{18}O_{SMOW}$ compositions of present-day rainwater at equivalent latitudes ($-3 < \delta^{18}O_{SMOW} < -5‰$ (Favara et al., 1998)) and a temperature of about 25–30 °C (tropical to sub-tropical).

*5.1.1. Host-rock*

The stable isotope signatures of host-rock samples (i.e. micrite dominated and bioclast-dominated) from Castelbuono and Cefalù have been analysed. Stable isotope values in samples from the Castelbuono quarry vary between −2.3 and −2.9‰ for $\delta^{18}O$ and between −0.2 and +0.3‰ for $\delta^{13}C$ (Fig. 7A). In Cefalù, the host-rock signature is more variable with $\delta^{18}O$ values ranging between −4.2 and −1.6‰ and $\delta^{13}C$ values ranging between −1.7 and +1.9‰. Most samples are slightly depleted with respect to reported signatures for Cenomanian marine carbonates (Voigt et al., 2003; Fig. 7A).

*5.1.2. Karst system*

$\delta^{18}O$ values from K-Cal-1 mainly vary between −8.0 and −2.0‰ whereas $\delta^{13}C$ values vary between −14.6 and 0.0‰ (Fig. 7A). The $\delta^{18}O$ values show a relatively large spread between −2.0 and −7.0‰ but the bulk of the analysed samples are in the range of −4.0 to −5.0‰ which is around the estimated value of the local meteoric water line (MWL) for the Panormide platform in Late Cretaceous time (Fig. 7A). The latter MWL was calculated using the stable isotope values of the calcite and on the assumption that precipitation occurred in equilibrium with temperatures currently occurring at latitudes similar to the estimated Late Cretaceous

palaeolatitude position of the Panormide platform (Stampfli and Borel, 2002).

The stable isotope values of K-Sed-1 range between −3.0 and −1.0‰ for $\delta^{18}O$ and between +1.0 and +3.0‰ for $\delta^{13}C$. K-Cal-2 that predates sedimentary infill is characterized by comparable values ($\delta^{18}O$ around −1.2‰ and $\delta^{13}C$ around +2.0‰). These values for K-Sed-1 and K-Cal-2 are in the range of typical marine signatures (Veizer et al., 1999).

All samples from diagenetic products in the karst cavities that postdate K-Sed-1 are characterized by carbon isotope signatures that vary with a few per mil below or above 0‰ (Fig. 7B). Samples from cavities where a high amount of bitumen was observed in the field have the lowest carbon isotope values, around −3‰. The $\delta^{18}O$ value of most diagenetic cements is depleted with respect to the typical marine signature (Veizer et al., 1999) (Fig. 7B). Considering the average $\delta^{18}O$ signature of K-Cal-4 (−6.0‰) and K-Cal-5 (−4.5‰), a slight increase of the $\delta^{18}O$ signature between these two diagenetic cements in the karst cavities is noted. Younger phases K-Dol-2 (−4.3‰) and K-Cal-6 (−7.2‰) record again a slight decrease in the $\delta^{18}O$ signature, taking into account the isotope fractionation between water and dolomite. The latter generates a dolomite value about 2–3 per mil larger than the coeval calcite (Land, 1980). K-Cal-6 is characterized by even higher $\delta^{18}O$ signatures that vary between −3.0 and +0.5‰. The stable isotope results from rhombic calcite samples are the most depleted with $\delta^{18}O$ signatures that reach −9.0‰.

### 5.1.3. High-angle faults

Carbon isotopes from cements within the fault zones are equivalent to normal marine carbon isotope signatures, mainly varying between +1.0 and +3.0‰ (Veizer et al., 1999) (Fig. 7C). Although the $\delta^{18}O$ signatures of F-Cal-1 samples from the Cefalù outcrop show a large spread (between −10.5 and −2.5‰), most results fall in the range of −4.0 and −6.0‰. In contrast, the few F-Cal-1 samples from the Castelbuono outcrop are characterized by completely different $\delta^{18}O$ signatures, varying between 0.0 and +2.0‰. F-Dol-1 and F-Dol-2 show a relatively large range in $\delta^{18}O$ values, varying between −8.5 and −2.5‰ (Fig. 7C). Only one sample from F-Dol-3 cement has been analyzed, due to the small size of these cements, its value being −5.8‰ for $\delta^{18}O$ and +1.7 ‰ for $\delta^{13}C$.

## 5.2. $^{87}Sr/^{86}Sr$ isotopes

All results from the Sr isotope analyses have been plotted in a $^{87}Sr/^{86}Sr$ – $\delta^{18}O$ cross-plot (Fig. 8). Since data couples for some samples are not available, boxes are used that indicate maximum and minimum variations of both variables for the different diagenetic products. The seawater variation curve has been plotted on this cross-plot, combined with a Mesozoic–Cenozoic time scale (McArthur et al., 2001). The presence of fossils suggest that K-Sed-1 is a marine sedimentary infill. Therefore, its age can be deduced from its $^{87}Sr/^{86}Sr$ isotope ratio (Burke et al., 1982). The $^{87}Sr/^{86}Sr$ isotope ratio of K-Sed-1 is more or less identical for each of the analysed samples and averages at 0.7078. The latter result agrees with a latest Cretaceous (±65 Ma) or Late Eocene age (±34 Ma), according to the $^{87}Sr/^{86}Sr$ secular variation curve of McArthur et al. (2001). K-Cal-4 has $^{87}Sr/^{86}Sr$ isotope ratios between 0.7081 and 0.7081. K-Cal-5, K-Dol-2 and rhombic calcite have $^{87}Sr/^{86}Sr$ isotope ratios in the range of 0.7077–0.7081. The results from calcite and dolomite samples occurring in the high-angle fault zones (F-Dol-1, F-Dol-2 and F-Cal-1) are well above the present-day value of seawater, i.e. values vary between 0.7095 and 0.7105 (see black rectangle in Fig. 8). Dolomitized fragments of the ancient host-rock are characterized by the lowest values whereas the dolomite in fractures is characterized by the highest signatures. Similar elevated $^{87}Sr/^{86}Sr$ ratios as seen in high-angle faults characterize K-Cal-6.

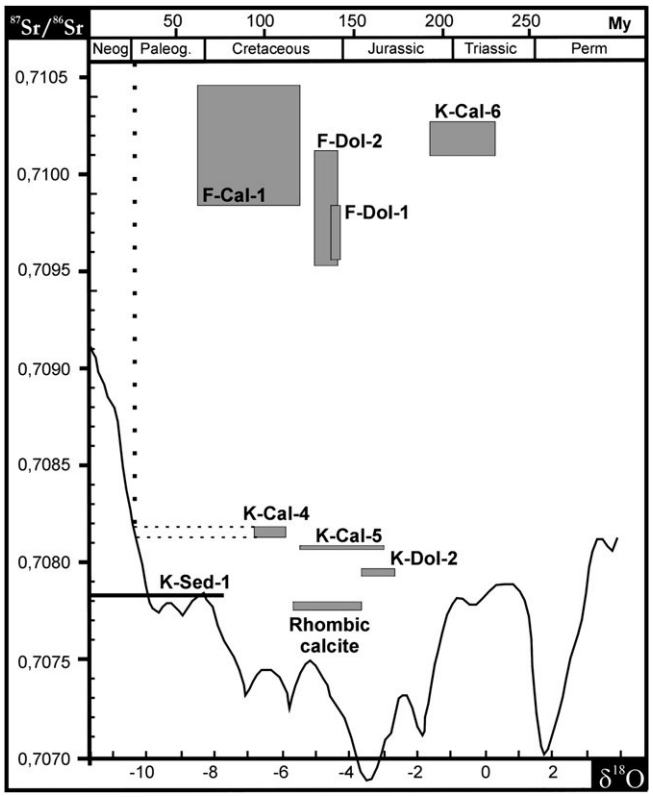


**Fig. 8.** $\delta^{18}O$–$^{87}Sr/^{86}Sr$ cross-plot with the $^{87}Sr/^{86}Sr$ signal of seawater through time (after McArthur et al., 2001). The thick part of this curve coincides with the measured age of the host-rock in Castelbuono and Cefalù. The horizontal black line shows the results for K-Sed-1 and where this result crosses the seawater variation curve. Since coupled data are not available for all the samples investigated, boxes are used that indicate maximum and minimum variations of both variables for the different diagenetic categories. The link between K-Cal-4 and timing that is discussed in the text is shown with dotted lines.

## 6. Fluid inclusions

The main petrographic characteristics and microthermometric data from the inclusions in the analysed diagenetic products (K-Cal-4, K-Dol-1, K-Cal-5, K-Dol-2 and K-Cal-7) are summarized in Table 1. The histograms for $T_m$ (last melting temperature) and $T_h$ (homogenization temperature) for each diagenetic phase are shown in Fig. 9.

### 6.1. Petrography

The only measurable inclusions were encountered in diagenetic phases precipitated in the karst system. Primary inclusions from K-Cal-4, K-Dol-1, K-Cal-5, K-Dol-2 and K-Cal-7 were measured. Secondary inclusions were only measured in trails in K-Cal-4. Diagenetic phases from within normal faults only had single phase inclusions (F-Cal-1) or where too small to do reliable observations and measurements (F-Dol-1 & F-Dol-2). Diagenetic phases from within the karst system often had well-developed crystals with growth zones in which primary inclusions could be recognized. The crystals were often not affected by crystal deformation. Both features are typical for crystals that have developed in open void space such as a karst cavity. Fluorite is the only diagenetic phase containing hydrocarbon inclusions, as shown by fluorescence

microscopy. The fluorite-contained hydrocarbon fluid inclusions have not been measured. Observed $T_{mi}$ in the different diagenetic phases is in line with the absence of gases in the inclusions such as $N_2$ or $CO_2$.

### 6.2. Microthermometric results

Based on the measured eutectic temperature ($T_e$), last melting temperature ($T_m$) and last melting temperature of hydrohalite ($T_{mhh}$), two different fluid types have been recognized, i.e. (1) a low saline fluid and (2) a high saline fluid with a $H_2O$–NaCl–$CaCl_2$ composition (Table 1 and Fig. 9). The low saline fluid presumably is composed of $H_2O$–NaCl although $T_e$ measurements are lacking to confirm such a hypothesis. The low saline fluid type occurs in primary inclusions from K-Dol-1, K-Cal-4, K-Cal-5 and K-Dol-2. Primary inclusions in K-Cal-6 and secondary inclusions in K-Cal-4 contain a fluid with a $H_2O$–NaCl–$CaCl_2$ composition. Using $T_m$ and $T_{mhh}$ measurements, it was possible to calculate the salinities (wt% NaCl and $CaCl_2$) of the fluids in inclusions with a $H_2O$–NaCl–$CaCl_2$ composition (Naden, 1993). For inclusions from which $T_e$ measurements are lacking, it was also possible to calculate the salinity (wt% NaCl), assuming a $H_2O$–NaCl composition of these inclusions (Bodnar, 1993). Fig. 10 summarizes the salinity data from the different phases in a wt% NaCl and wt% $CaCl_2$ cross-plot. There are slight differences in $T_m$ data for inclusions typified by a $H_2O$–NaCl system. K-Dol-1 is characterized by very low $T_m$ whereas primary inclusions in K-Cal-4 show slightly more elevated $T_m$ values which more or less coincide with the salinity of present-day seawater. Both K-Cal-5 and K-Dol-2 are characterized by very low $T_m$ data (Table 1).

There is a lot of variation in the measurements of homogenization temperatures from fluid inclusions in different diagenetic phases. $T_h$ of K-Dol-1 is characterized by a very broad range which likely relates to stretching because inclusions from three crystals have been measured and the results differ for each crystal. One crystal was stretched during measurement. This was attested by the difference between primary data (characterized by $T_h$ values between 70 and 100 °C) measured before stretching and secondary data (characterized by $T_h$ values above 130 °C) measured after stretching. The second crystal shows $T_h$ values all above 130 °C. The other crystal is characterized by a normal distribution around $T_h$ of 90 °C with a tail of higher $T_h$ temperatures, a feature commonly interpreted as stretching (Goldstein and Reynolds, 1994). The few measured primary inclusions in K-Cal-4 are more or less characterized by the same $T_h$ as the unstretched inclusions in K-Dol-1. The $T_h$ of secondary inclusions varies between 70 and 200 °C with a mean around 120 °C (Fig. 9). K-Cal-5 and K-Dol-2 show more or less the same normal distribution with mean $T_h$ around 140 °C. Maximum and minimum values are also more or less identical. The $T_h$ measurements in K-Cal-6 (130–180 °C) are quite high. During repeated heating experiments on the same inclusion, it was noted that the gas bubble changed its size considerably. On other occasions, inclusions in K-Cal-6 showed leakage with increasing bubble size or even explosion during heating experiments. Interpretation of the temperature data from inclusions in K-Cal-6 is thus equivocal (Goldstein and Reynolds, 1994).

## 7. Interpretation

The available petrographic, geochemical, microthermometric and structural data allow constructing the paragenesis in the karst system and interpreting the nature and origin of the diagenetic products. The discussion (see below) will then focus on the fluid flow reconstruction and how the fluid flow history is related to the burial and kinematic history. Crosscutting, but mainly overgrowth relationships between diagenetic products in the karst system were used to build the paragenesis. The order in which the diagenetic products have been described above roughly reflects already the relative timing of different diagenetic events. From crosscutting relationships, it is obvious that the karst system formed prior to the normal faults that crosscut cavities and connecting dissolution enlarged fractures. Therefore, the diagenetic products in the karst system are interpreted first.

K-Cal-1 directly grows on the cavity walls and is the first phase precipitated in the karst system. K-Cal-1 most likely reflects precipitation from meteoric fluids in a karst environment. Petrographic aspects such as the lamination in the calcite cements lining the cavities and the alternation of elongate blocky and scalenohedral equant calcite are largely comparable to present-day speleothems (Railsback et al., 1994). Furthermore, the zoned cathodoluminescence pattern in K-Cal-1 suggests changing $E_h$ conditions that typically exist in diagenetic environments where surface and subsurface waters are in contact (Machel and Burton, 1991). The petrographic evidence for meteoric fluid flow during K-Cal-1 precipitation is further supported by geochemical evidence. The relatively low carbon isotope values of K-Cal-1 can be explained by precipitation in a meteoric environment due to the involvement of soil-derived $CO_2$ (Allan and Matthews, 1982; Anderson and Arthur, 1983; Lohmann, 1988). In addition, the $\delta^{18}O$ values of K-Cal-1 cements cluster around the local ancient Cretaceous MWL, even though there is a relatively large spread (Fig. 8A). The latter is likely the result of recrystallization during later stages in the fluid flow history, as suggested by the patchy luminescence pattern encountered in some of the K-Cal-1 cements (Fig. 5C). Both cold and hot marine fluids that later migrated through the karst system (see below) might have played a role in the recrystallization. Respectively, they could have increased or decreased the $\delta^{18}O$ signature of K-Cal-1. Alternative explanations to the patchy luminescence and variable $\delta^{18}O$ values of K-Cal-1 include contamination from the host-rock in the analysed samples or from later authigenic phases.

Sediment infill by K-Sed-1 postdates K-Cal-1 precipitation in the karst system (Fig. 4). Overgrowth relationships indicate the occasional presence of columnar K-Cal-2 cement in between K-Cal-1 and K-Sed-1. K-Cal-2 and K-Sed-1 are interpreted to be respectively

**Table 1**
Summary of the petrographic characteristics and microthermometric results from fluid inclusions enclosed by the Castelbuono and Cefalù diagenetic phases.

| | Inclusion size (μm) | Vapour ratio (%) | Number of phases | Occurrence | $T_{fm}$ (°C) | $T_h$ (°C) | $T_m^{ice}$ (°C) | $T_m^{hh}$ (°C) |
|---|---|---|---|---|---|---|---|---|
| K-Dol-1 | 3–20 | 5–10 | Mono & bi | Primary growth zones | ? | 60 to −180 | −1.9 to −1.3 | – |
| K-Cal-4 primary inclusions | 2–9 | 10–20 | Bi-phase | trails in growth zones | −51 to −49 | 80.6 to 127.2 | −5.4 to −1.6 | – |
| K-Cal-4 secondary inclusions | 5–50 | Variable | Mono & bi | Secondary trails mainly along cleavage | −52 to −47 | 65.8 to 196 | −11.9 to −5.4 | −24.6 to −22.3 |
| K-Cal-5 | 2–6 | ±10 | Bi-phase | Primary growth zones | ? | 100 to 180 | −2.4 to −0.4 | – |
| K-Dol-2 | 5–10 | 5–15 | Mono & bi | Primary growth zones | ? | 116 to 164 | −2 to −0.4 | – |
| K-Cal-6 | 5–70 | Variable | Mono & bi | Primary growth zones | −53 to −46 | 100 to 180 | −16.8 to −9 | −27.4 to −21.6 |

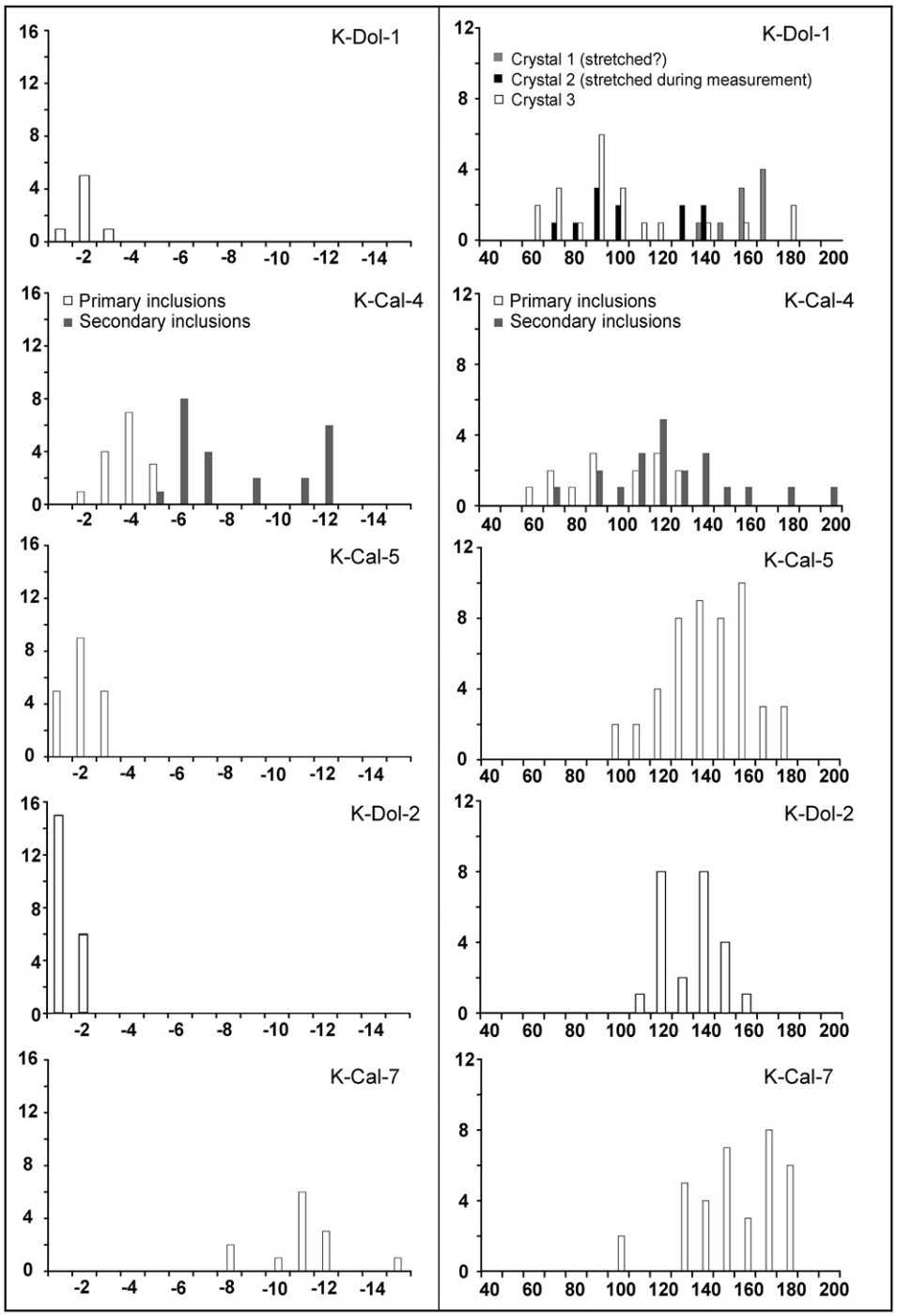


**Fig. 9.** Left column: summary of the $T_m$ data (°C) from the different inclusion types analysed. Right column: summary of the $T_h$ data (°C) from the different inclusion types analyzed. In all histograms, vertical axis indicates the number of measurements ($n$) and horizontal axis is temperature ($T$).

precipitated and sedimented in a marine diagenetic environment. This interpretation is based on their stable isotope results that typically fall in the marine range, the presence of nannofossil assemblages in K-Sed-1 and the columnar shape of K-Cal-2, typical for calcite precipitating under marine conditions (Moore, 2001). The presence of large amounts of sediment infill as well as the non-luminescent character of K-Cal-2 supports sedimentation and precipitation in oxidizing conditions, close to the sediment-water contact (Machel and Burton, 1991).

The precipitation of K-Cal-4 followed K-Sed-1 sedimentation and marks a change in the diagenetic environment. The oxygen stable isotope signatures are depleted with respect to the typical marine oxygen isotopic compositions of K-Sed-1. Nevertheless, measured salinity of the primary inclusions in K-Cal-4 (3.14–6.09 wt% NaCl) is equivalent to double the salinity of seawater (3.2 wt% NaCl). The depletion in $\delta^{18}O$ signature is attributed to temperature fractionation since homogenization temperatures of up to 100 °C have been measured in primary inclusions from K-Cal-4. In fact, based on the relationship between the precipitation temperature as inferred from homogenization temperatures (60–100 °C) and the $\delta^{18}O$ values of the precipitated calcite (−7.0 to −6.0‰), a $\delta^{18}O$ of −1.0 to +1.0‰ V-SMOW can be calculated for the original fluid using

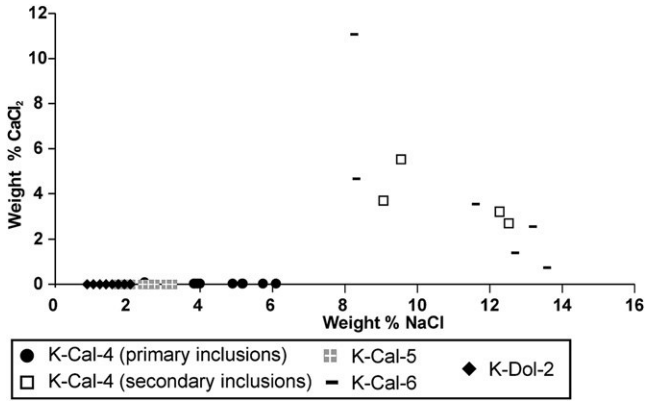


**Fig. 10.** Summary on the composition of fluid inclusions from different diagenetic phases in a wt% NaCl–wt% $CaCl_2$ cross-plot.

equations from O'Neil and Epstein (1969) and Friedman and O'Neil (1977). The relatively large spread in measured homogenization temperatures might indicate precipitation at increasingly higher temperatures. The evidence thus suggests that K-Cal-4 precipitated from marine or marine-derived pore fluids during gradual burial. It is likely that an open system existed between the permeable karstified limestones and the overlying Numidian flysch sandstones at relatively shallow burial depths when compaction of the sandstone bodies was minimal.

K-Cal-3 and K-Dol-1 are two diagenetic phases that occur relatively rare and for which the origin and nature as well as the timing are uncertain. A limited number of overgrowth relationships indicate that K-Cal-3 formed after K-Sed-1 but prior to K-Cal-4 precipitation. Crystal stratigraphy with cathodoluminescence varying from non- over bright to dull luminescence supports precipitation during early stages of burial, where $E_h$ conditions change from oxidizing to reducing.

K-Dol-1 predates K-Cal-4 but more precise determination of its timing is not possible. The dolomite was only encountered in two samples and detailed overgrowth relationships with K-Cal-1, K-Sed-1, K-Cal-2 and K-Cal-3 are lacking. The Fe-poor nature of K-Dol-1 and the comparability between $T_h$ of K-Dol-1 and K-Cal-4 suggests that both phases are more or less contemporaneous or that $T_h$ of K-Dol-1 has been reset by K-Cal-4 fluids. The salinity in K-Dol-1 inclusions is slightly lower than the salinity of primary inclusions in K-Cal-4 and than the salinity of seawater. This is in line with dolomite formation in a mixing zone situation (Badiozamani, 1973). However, too little is currently known to draw any definite conclusions with regard to the origin of the dolomite cement. Geochemical analysis of K-Dol-1 was impossible since the size of the dolomite crystals prevents sampling without contamination by other diagenetic phases.

Fe-rich K-Cal-5 overgrows K-Cal-4 but also occurs in fractures crosscutting K-Cal-4 cement. K-Cal-5 cement in turn predates fluorite precipitation (K-Fl-1). The fluorite precipitation is associated with hydrocarbon migration, as shown by the presence of green fluorescent two-phase hydrocarbon inclusions in the fluorite crystals. In addition, bitumen has been encountered in several samples, always overlying K-Cal-5. An Fe-rich saddle dolomite phase (K-Dol-2) grows on top of the bitumen. Microthermometric and geochemical results suggest that K-Cal-5 and K-Dol-2 are precipitated from the same Fe-rich and low saline fluid type at relatively high homogenization temperatures ($T_h$ in the range of 120–180 °C). In comparison with earlier diagenetic phases (K-Cal-4), a shift towards higher homogenization temperatures is observed for K-Cal-5 and K-Dol-2 in combination with enrichment by +1.0 to +2.0‰ for average oxygen isotope values. Given that temperature fractionation generally lowers average oxygen isotope values at higher precipitation temperatures, the results indicate that the low saline fluids where enriched in $^{18}O$ relative to earlier marine-derived fluids. Calculating the $\delta^{18}O_{SMOW}$ values of original fluids in equilibrium at the range of temperatures obtained in fluid inclusions (120–180 °C), a $\delta^{18}O_{SMOW}$ composition between +6.0 to +14.0‰ is envisaged. Such a positive $\delta^{18}O$ signature excludes the involvement of meteoric fluids but typifies formation waters (Sheppard, 1986). Most commonly, the low salinity of such fluids is related to the diagenetic or metamorphic dehydratation of certain minerals (e.g. smectite–illite transformation) (Dahlmann and de Lange, 2003; Kastner and Le Pichon, 1992; Larroque et al., 1996; Sheppard, 1986; Taylor, 1990).

According to the overgrowth relationships in the karst system, hydrocarbon migration associated with fluorite precipitation, took place after K-Cal-5 but prior to K-Dol-2 precipitation. No hydrocarbon inclusions were encountered in K-Cal-5 or K-Dol-2, showing that hydrocarbon migration was not taking place during their precipitation. Therefore, the available petrographic information supports one single event of hydrocarbon migration through the karst system. Fluorite precipitation associated with hydrocarbon migration is relatively common throughout the geological history (e.g. Benchilla et al., 2003). The possible sources for hydrocarbons will be discussed below.

K-Cal-6 is the last diagenetic phase encountered in the karst system. This phase is again Fe-poor and is characterized by an increased $^{87}Sr/^{86}Sr$ isotope ratio relative to all previous phases in the paragenesis. Microthermometric results show that the fluids responsible for the precipitation of K-Cal-6 are still at elevated temperatures comparable to homogenization temperatures for K-Cal-5 and K-Dol-2. However, the salinity of the fluids has changed completely with the presence of high saline fluid inclusions. At the same time, $H_2O$–NaCl fluids occurring in K-Cal-5 and K-Dol-2 were also replaced by $H_2O$–NaCl–$CaCl_2$ in the fluid inclusions. K-Cal-6 thus reflects the influx of high saline and hot fluids into the karst system.

The diagenetic products encountered in the high-angle faults (F-Dol-1, F-Dol-2 and F-Cal-1) have similar geochemical characteristics as K-Cal-6 with elevated $^{87}Sr/^{86}Sr$ isotope ratios and all are Fe-poor. Unfortunately, it was impossible to study fluid inclusions in dolomite or calcite precipitated in the high-angle fault system since they were too small and mostly single phase. Hence, the salinity of the fluids migrating along the high-angle faults could not be directly compared to the high salinity encountered in K-Cal-6 fluid inclusions.

Note that rhombic calcite has been omitted in the interpretations above. Because this phase overgrows bitumen droplets (Fig. 4E), it is certain that it postdates oil migration. The low $^{87}Sr/^{86}Sr$ isotope ratio of rhombic calcite shows that the rhombic calcite precipitated from different fluids than K-Cal-6. However, the absence of reliable microthermometric data from this phase makes it impossible to further constrain the timing and origin of the fluids.

Whereas the carbon isotope values of K-Cal-1–K-Cal-3 display typical marine signatures (+1 to +3‰), the carbon isotope values of younger carbonate diagenetic phases in the karst system, with the exception of K-Cal-6, are slightly more depleted with values ranging between −3.0 and +1‰ (Fig. 7A,B). Lowest carbon isotope signatures are observed in cavities with abundant bitumen present. Carbon isotope depletion is typical for fluids that have been in contact with maturing organic matter that preferentially consists of $^{12}C$ (Allan and Matthews, 1982). Since fluids responsible for the precipitation of K-Cal-4 are thought to come from Oligocene flysch units, black shales contained in these units could have played a role in lowering the carbon isotope signature of K-Cal-4 (Granath and Casero, 2004). Since K-Dol-2 and K-Cal-5 precipitated from fluids that migrated more or less at the same time as hydrocarbons, it

could well be that the aqueous fluids interacted with maturing organic material. Other explanations regarding the depletion of carbon isotope values include contamination of the carbonate samples used for analysis by bitumen or recrystallization of carbonate minerals after precipitation and in contact with mixtures of aqueous and organic fluids. The latter is not supported by any observed cathodoluminescence textures in the crystals that could point to recrystallization. The former is not unlikely since samples were not cleaned for hydrocarbon removal prior to reaction and analysis. Furthermore, bitumen in the cavities is spatially closer to younger carbonate phases, making contamination during micro-drill sampling more likely.

## 8. Discussion

### 8.1. Fluid flow history

The paragenesis only represents the relative timing of the different diagenetic events. The true value in fluid flow reconstruction comes with linking the paragenesis to a fluid flow history that can be placed in a regional kinematic and burial history framework (Figs. 11 and 12). The discussion will focus on the latter exercise in the study area. Furthermore, implications from the present study for hydrocarbon exploration will be discussed.

From the paragenesis and the interpretation of the geochemical and microthermometric results, a fluid flow history with five stages can be deduced (Figs. 11 and 12). The subdivision in five stages is based on four major changes that occurred in the geochemical or microthermometric signal of diagenetic products at certain stages in the paragenesis. These changes indicate the start of a new stage in the fluid flow history.

#### 8.1.1. Stage 1: karstification by meteoric fluids

The first fluid stage recorded in the karst system by K-Cal-1 is meteoric in origin. Moreover, the karst system itself is most likely created by the same meteoric fluids during emergence of the Panormide platform. The position of the karst system, just below the major regional unconformity with palaeotopography, makes

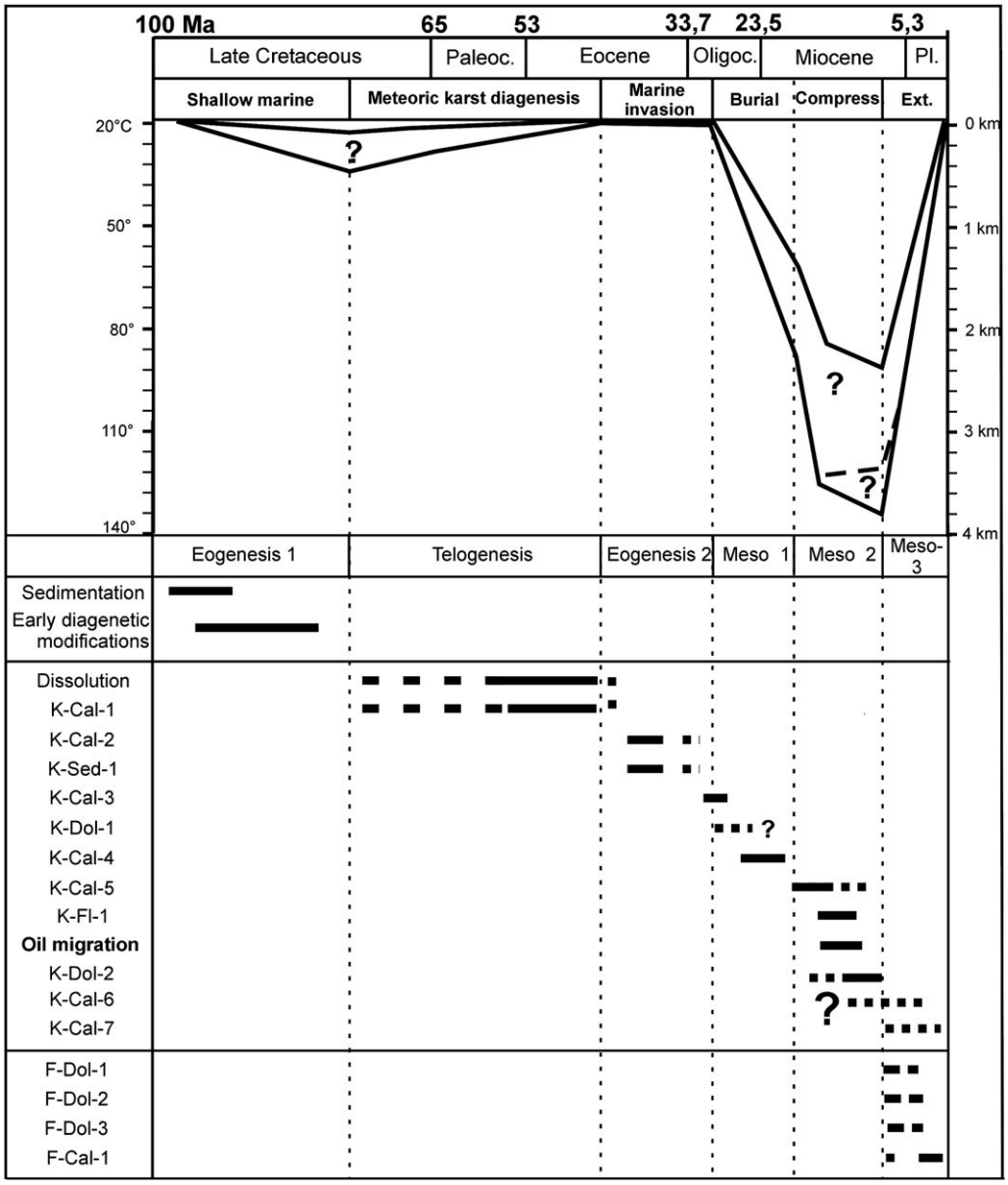


**Fig. 11.** Paragenesis linked to the burial history and the geological evolution of the study area (for explanation, see text).

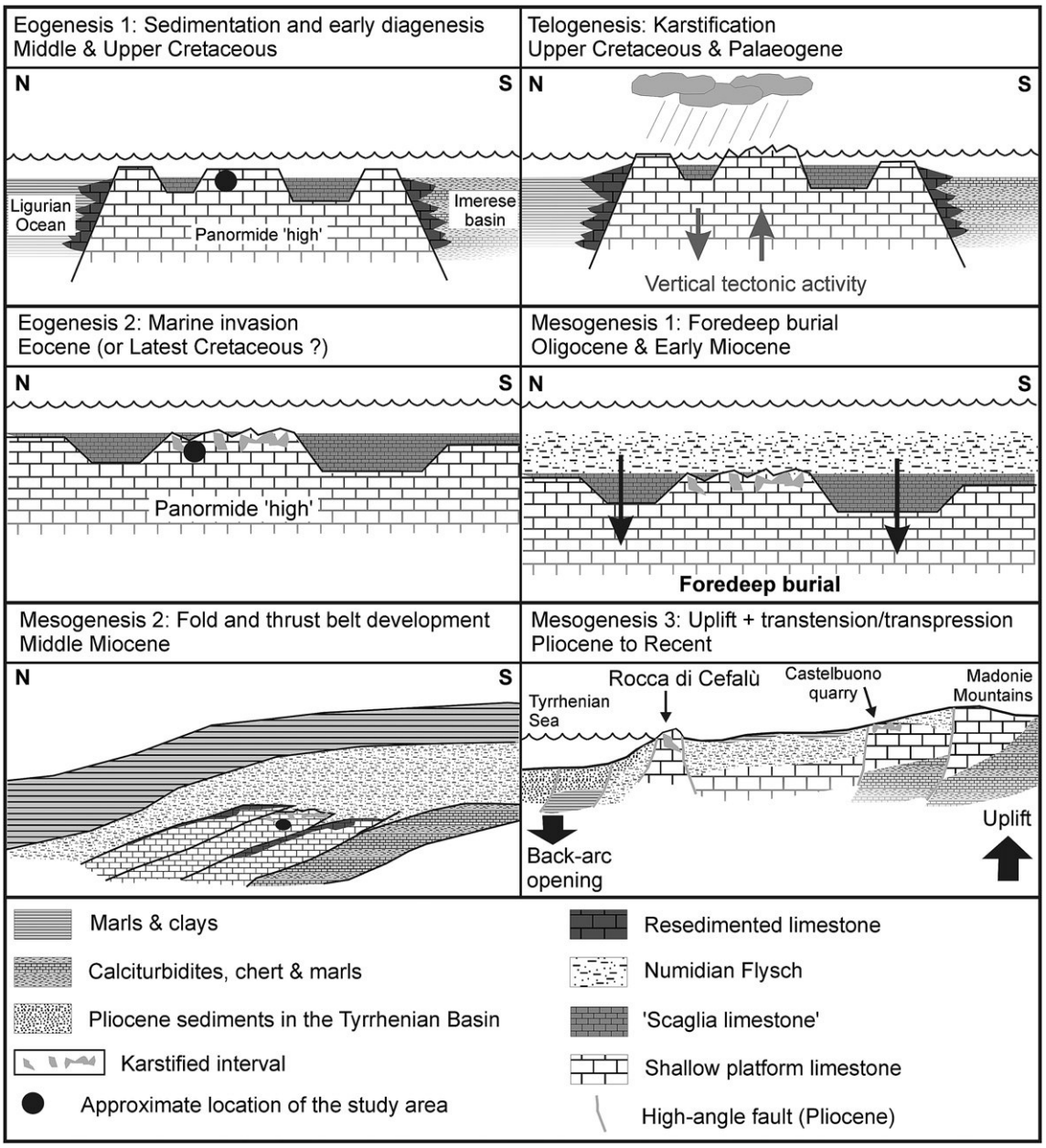


**Fig. 12.** Schematic representation of the kinematic and fluid flow history of the Cretaceous units in the Panormide domain of north-central Sicily from the Cretaceous up to now. The drawing (upper left) shows the geological setting in the Cretaceous with the Panormide 'high' flanked by the Ligurian Ocean to north and the Imerese Basin to the south. Sedimentation in the Panormide domain during the Cretaceous was heterogeneous and consisted of contemporaneous pelagic and shallow platform sedimentation. Pelagic sedimentation prevailed in the Ligurian Ocean and the Imerese Basin with resedimentation of carbonate debris alongside the flanks of the Panormide high. The black dot marks a possible position for the Cefalú–Castelbuono study area. The upper Drawing shows the emergence of part of the platform and the resulting infiltration of meteoric water, responsible for the karstification. The arrows indicate the vertical tectonic movements that were likely the cause for emergence. The middle left drawing is an enlargement of the previous drawing where the platform is submerged again and represents the time when marine sediments invade the karst system. Zooming out again in the middle right, this drawing represents foredeep burial and Oligocene–Miocene Numidian flysch sedimentation while thrusting has started in the north. Zooming out even further in the lower left drawing, full fold and thrust belt development took place in the Middle Miocene. The Panormide units were buried under marls and clays from the Sicilide units and thrusting progressed from north to south. In the last stage of the flow history (lower right drawing), fluid flow was especially focused along high-angle faults that developed during the opening of the Tyrrhenian back-arc basin and the uplift of the Madonie Mountains.

the possibility that the karst system was formed in a coastal mixing zone system or by hydrothermal fluids unlikely. Due to dissolution of the limestone during karstification, meteoric fluids eventually became saturated with calcite and precipitated K-Cal-1 that is closely associated with cavity walls and dissolution enlarged fractures. Similar karstified limestones from Cretaceous age occur throughout Italy and elsewhere in the Mediterranean and serve as hydrocarbon reservoirs (e.g. Andre and Doulcet, 1987; Anelli et al., 1996; Roure et al., 2004). Emergence and karstification of these shallow water platforms in the same era is often related to vertical tectonic activity during the onset of Alpine deformation in the Mediterranean (Di Stefano et al., 1996).

### 8.1.2. Stage 2: marine invasion

The start of stage 2 in the fluid flow history is marked by the precipitation of K-Cal-2 and the sedimentation of K-Sed-1 into cavities of the karst system. Both are clearly marine in origin and indicate that meteoric fluid flow and emergence were finished and

that marine fluids circulated in the karst system at this stage. The exact timing of the marine invasion and K-Sed-1 sedimentation in the karst reservoir remains speculative. The nannopalaeontological data indicate that marine sediment was being introduced into the karst system as early as the Late Campanian. This would imply a relatively short period of meteoric fluid flow and karstification, much shorter than implied by the stratigraphic gap between the Late Cretaceous limestones and the Oligocene Numidian flysch at the regional unconformity. A Late Cretaceous age also complies with the $^{87}Sr/^{86}Sr$ isotope data from K-Sed-1 (McArthur et al., 2001).

The general petrographic characteristics of K-Sed-1 in the karst cavities are very similar to the 'scaglia' sediment in the region that is of latest Cretaceous to Eocene age (Lentini and Vezzani, 1974; Miuccio et al., 2000). This thin 'scaglia' sediment occurs in a patchy nature throughout the study area, often associated with small depressions in the palaeotopography (pers. comm. Di Stefano). The fine-grained pelagic sediment likely penetrated the karst cavities, suspended in the marine fluids that circulated there.

Nowhere in the field or in any of the samples, macroscopic or microscopic overgrowth relationships indicate an alternation between meteoric and marine fluid circulation, suggesting alternation between respectively emergence and submergence of the shallow water platform. Therefore, a single stage of karstification followed by submergence of the platform is assumed. Even though a limited number of samples were analysed with nannopalaeontology and Sr isotopes, the dating of the sediment infiltration as latest Cretaceous represents an important link of the relative paragenetic timing with the absolute time scale (Fig. 11).

#### 8.1.3. Stage 3: heating of marine fluids during foredeep burial

The start of stage 3 coincides with precipitation of K-Cal-4. The latter is still precipitated by marine fluids as shown by measured salinities equal or slightly higher than that of seawater. However, the elevated homogenization temperatures in primary inclusions and a depleted $\delta^{18}O$ signature with respect to the typical marine signature are enough reason to define a new stage in the fluid flow history. Using the $^{87}Sr/^{86}Sr$ isotope ratio and assuming the marine fluid is pristine, it can be estimated that K-Cal-4 has a Late Oligocene age, between 25.35 and 24.25 Ma (McArthur et al., 2001; Fig. 8). The range in homogenization temperatures is equivalent to a burial of 1.5–2.5 km which is more or less the estimated thickness of the time-equivalent Numidian flysch series in the region (Brocquet, 1970; Lentini and Vezzani, 1974). All these observations suggest that K-Cal-4 precipitated from marine or marine-derived fluids during foredeep burial when thick series of Numidian flysch were deposited on top of the unconformity and the underlying karst reservoir. There is no evidence of active marine fluid circulation. Probably, Oligocene marine fluids were stored in the karst reservoir and were gradually heated during foredeep burial. The slightly elevated salinities with respect to seawater could be the result of water–rock interactions between the original interstitial seawater and the carbonate rocks.

Crosscutting relationships between K-Cal-3 and K-Cal-4 do not exist. The cathodoluminescence pattern of the crystals reflects precipitation during a transition from oxidizing to reducing conditions (non-, bright, and dull) (Machel and Burton, 1991). Therefore, it is proposed here that K-Cal-3 was precipitated during the early stages of foredeep burial (Fig. 11) but geochemical evidence to proof this hypothesis lacks.

The origin of the relatively rare K-Dol-1 crystals in this perspective is uncertain. Measured salinities of the fluid inclusions in K-Dol-1 show that fluids were slightly less saline than marine fluids encountered in K-Cal-4, suggesting a mixing zone dolomitization event. Given that the place of K-Dol-1 in the paragenesis is uncertain due to the lack of clear overgrowth relationships, it is proposed that K-Dol-1 precipitated somewhere before the onset of burial, possibly in between stages 2 and 3.

#### 8.1.4. Stage 4: expulsion of hot and low saline fluids and hydrocarbon migration

A new stage in the fluid flow history was defined because hot fluids were introduced into the karst reservoir with salinity lower than seawater, as shown by the microthermometric data for K-Cal-5 and K-Dol-2. Stage 4 entails the precipitation of K-Cal-5, hydrocarbon migration and precipitation of fluorite and K-Dol-2.

Low saline fluids generally originate from the influx of meteoric water or from dilution processes, of which most common examples are dehydratation of clays such as smectite and the liberation of water during metamorphism. Calcite or dolomite precipitated from hot meteoric fluids would generally generate rather depleted $\delta^{18}O$ signatures. This is not the case for K-Cal-5 and K-Dol-2 which both are characterized by slightly increased $\delta^{18}O$ signatures compared to K-Cal-4. Therefore, it is proposed that low saline fluids were introduced in the reservoir from somewhere outside the Cretaceous limestone reservoir rocks. The presence of fluorite and hydrocarbons further evidences an external source for fluid flow during stage 4 of the fluid flow history.

The exact origin of the fluids remains more speculative and possibly is a mixture of local and external fluids. The relatively high $\delta^{18}O$ signatures and the ferriferous nature of the precipitated carbonate minerals favours a model in which at least part of the fluids was generated during clay-related diagenetic reactions such as smectite–illite conversion (Boles and Franks, 1979; Sheppard, 1986; Taylor, 1990). However, dilution by clay diagenetic or metamorphic reactions would generally increase the $^{87}Sr/^{86}Sr$ ratio in the fluids and in any diagenetic product precipitating out of them (Moore, 2001; Stueber et al., 1984). Possible explanations for anomalous low $^{87}Sr/^{86}Sr$ ratio of K-Cal-5 and K-Dol-2 could be found in the interaction with volcanic ash or underlying oceanic crust (Dia et al., 1995) or could have been caused by mixing of different fluid types. The latter phenomenon is typical in complex basinal settings (e.g. Bachu, 1997; Connolly et al., 1990; McCaig et al., 2000). Homogenization temperatures in excess of 160 °C were measured in K-Cal-5 and K-Dol-2 fluid inclusions. There is no stratigraphic evidence that foredeep burial reached a depth deep enough to generate such high temperatures in equilibrium with burial. Therefore and because of the external origin of the fluids, it is postulated that the hot and low saline fluids were expulsed during Middle Miocene compressional tectonic deformation after the foredeep burial.

If the hypothesis regarding expulsion of fluids during compression is correct and with a south to southwest propagation of the FTB, the source area of the fluids was most likely located north of the study area. Keeping in mind the low salinity of the fluids, the most likely source are shale and marl units from the Sicilide units that have been dewatered during compressional deformation. Especially thrusts are known conduits for expulsion of fluids towards the foreland during compressional deformation (e.g. Oliver, 1986; Moore and Vrolijk, 1992). Geochemical and microthermometric results from Dewever et al. (2006) and Larroque et al. (1996) in more southern units in Sicily suggest the presence of hot low saline advective fluid flow along major décollements in the fold and thrust belt. These authors have studied diagenetic products occurring in a thrust zone and measured homogenization temperatures up to 180 °C in low saline fluid inclusions. The presence of high amounts of manganese in calcite showed that the fluids were most likely generated during clay diagenetic transformations. Unfortunately major thrust faults that would allow comparing potential fluid flow in a thrust fault with that during stage 4 of the fluid flow history in the karst system are not exposed in the study area.

Paragenetic relationships indicate that hydrocarbon migration and fluorite precipitation occurred after K-Cal-5 but prior to K-Dol-2 precipitation. The latter are so similar in geochemical characteristics that a similar fluid source was postulated. Therefore, it is not unimaginable that the hydrocarbons were sourced from the same units from which hot and low saline fluids were expulsed. However, proof for such a hypothesis is lacking. The $\delta^{13}C$ signatures of K-Cal-5 and K-Dol-2 are not depleted. The latter could be expected when $CO_2$ derived from the maturation of organic matter would be involved in the precipitation of carbonates. The hydrocarbon migration and its possible source rocks will be discussed in more detail in Section 8.2.

#### 8.1.5. Stage 5: high saline and radiogenic fluid flow during normal fault development

The onset of stage 5 in the fluid flow history of the karst system is marked by the influx of Fe-poor and high saline fluids, replacing the Fe-rich and low saline fluids from stage 4. Furthermore, there is a clear change in the composition of the fluid inclusions, indicated by measured $T_{mi}$ temperatures. Up to now, fluids were typified by a simple $NaCl–H_2O$ system. With stage 5, fluids with a $NaCl–CaCl_2–H_2O$ composition enter the karst system.

Stage 5 of the fluid flow history is most likely linked to normal fault development in the region which resulted of the collapse of the Sicilian fold and thrust belt in the Pliocene (Catalano et al., 1996; Giunta et al., 2000a). The diagenetic products from stage 5 in the karst system have the same petrographic (Fe-poor) and geochemical signature (elevated $^{87}Sr/^{86}Sr$ isotope signature) as the diagenetic products encountered in the normal faults. Similarity in $\delta^{18}O$ signature is less obvious due to the wide range of values encountered in the karst system as well as in the normal faults. K-Cal-6 in the karst system is generally characterized by slightly less depleted $\delta^{18}O$ values ($-2.8$ to $0.3‰$) with respect to K-Cal-5 and K-Dol-2 precipitated during stage 4. Note that all the K-Cal-6 samples from within the karst system were taken in the quarry in Castelbuono. Even higher and slightly positive $\delta^{18}O$ values (0 to $+2‰$) are reported for calcite from within fault zones in Castelbuono. Calcite in faults at Cefalù is characterized by a more depleted $\delta^{18}O$ signature ($-3$ and $-10.5‰$). This suggests a very local control on the $\delta^{18}O$ signature of carbonates precipitated during stage 5. The latter could be the result of different fluid–rock interactions, variable physico-chemical conditions during precipitation, changing rates of fluid mixing, different fluid types being tapped in different faults or a combination of two or more of these factors.

From all the observations and measurements performed on diagenetic products classified as pertaining to fluid flow stage 5 in normal faults as well as in the karst system, it is difficult to gather a clear image of the origin of the fluids. The constant elevated $^{87}Sr/^{86}Sr$ isotope ratios in all samples from the karst system and the normal faults show that a siliciclastic-derived component is present at the regional scale. The extended range of measured homogenization temperatures can be explained by a number of causes, i.e. (1) temperature fractionation; (2) mixing of different fluids at different ratios; and not least (3) incorrect measured homogenization temperatures. The observed instability during heating experiments supports hypothesis (3) and rules out any further interpretations to be done on the measured homogenization temperatures. The high salinities observed in measured fluid inclusions from K-Cal-6 can also be attributed to different fluid types. Deep formation waters are generally relatively saline due to water–rock interactions. A system with percolating rain water, interacting with Messinian evaporites could also be envisaged. The fluids would greatly increase their salinity due to water–rock interactions and then percolate deeper into the sediments, migrating preferentially along high-angle faults. Unfortunately, salinities from K-Cal-6 in the karst system could not be compared to fluid inclusion results from calcite or dolomite in high-angle faults. Nevertheless, it can be proposed that comparable high saline fluids were necessary to provoke dolomitization in a rim zone along faults (e.g. Gasparrini et al., 2006; Warren, 2000). Although not immediately evident from the geochemical data, shallow marine fluids might also have played a role during stage 5 of the fluid flow history. Downward infiltration of such fluids could explain the sandy infill in certain high-angle fault zones. In summary, it is very likely that fluids from different sources mixed during stage 5 of the fluid flow history in high-angle fault zones as well as in the karst system.

### 8.2. Implications for hydrocarbon exploration

The results of the present study have implications for hydrocarbon exploration and prospectivity in this part of the Sicilian fold and thrust belt. Even though the reservoir properties of the karstified limestone were not the primary subject of the present study, the study identifies the Middle and Late Cretaceous Panormide limestone as a potential prospective reservoir unit in the Sicilian FTB. Abundant secondary vuggy porosity was created during karstification. In the study area, most of this porosity has been occluded by later karst infill in the form of sedimentation or diagenetic precipitation. It is uncertain at the regional scale how much of the Panormide domain was affected by karstification. The vertical tectonic activity, responsible for emergence and submergence of certain areas was probably very heterogeneous. The compilation of a detailed Cretaceous palaeogeographic facies map of the Panormide domain would help in identifying regions where shallow and/or emerged conditions could have occurred, i.e. where reservoir conditions could have developed. Interestingly, the setting of this potential reservoir below a major regional unconformity between Cretaceous limestones and Oligocene to Miocene foredeep sediments is not unique for Italy (Anelli et al., 1996). The Rospo Mare field offshore in the Adriatic foredeep produces from karstified Cretaceous limestones that occur in a similar tectono-stratigraphic setting, just below a major regional unconformity between Upper Cretaceous platform limestones and foredeep flysch deposits (Andre and Doulcet, 1987; Soudet et al., 1994). In contrast with the studied rocks in Sicily, the Adriatic equivalents have not yet been affected by compressional tectonic activity during Apennine–Maghrebian tectonics. The comparability of both scenarios suggests the importance of Cretaceous karstified limestones on a broader scale in the Central and western Mediterranean region.

The timing of oil migration in the Sicilian FTB has always been a matter of debate (Granath and Casero, 2004). Therefore, an interesting result with respect to hydrocarbon exploration in the Sicilian fold and thrust belt relates to the relative constraints that have been put on the timing of oil migration. Coupling the fluid flow history to the kinematic and burial history unambiguously shows that hydrocarbon migration occurred either during foredeep burial or more likely, during thrust emplacement. Furthermore, the hydrocarbons were probably expulsed from the thrust front into the foreland. This is comparable to what Larroque et al. (1996) have proposed in relation to hydrocarbon migration at the toe of the Sicilian wedge. Of course, it cannot be ruled out that earlier phases of hydrocarbon migration occurred in the region, prior to the sedimentation of the Late Cretaceous karstified limestones. The potential source rock that could have sourced the hydrocarbons remains highly speculative. If the hydrocarbons were truly expulsed from the thrust front into the foreland, the source rock should have been located north of the Panormide platform. Granath and Casero (2004) indicate the presence of a potential source rock

interval in this region, i.e. Late Jurassic–Early Cretaceous marls and limestones from the Sicilide units. It is possible that these units generated the oil, together with hot and low saline fluids, during compressional tectonic activity and thrust emplacement. However, siliceous shales of the Crisanti Formation that have been deposited in the Imerese basin south of the Panormide platform should not be overlooked (pers. comm. Prof. F. Roure). Such siliceous shales represent the equivalent of the source rocks that have sourced the producing on- and offshore carbonate reservoirs in the Hyblean foreland of Sicily.

Finally, the timing of oil migration indicates that foredeep burial and or tectonic burial have been necessary to mature the unknown source rock. This is an important observation for future exploration. It shows that hydrocarbon migration routes were most likely controlled by tectonic features. This is not only documented at the toe of the Sicilian wedge (Larroque et al., 1996) but also at Monte Kumeta where oil seeps occur in the fault zone of the regional strike-slip Kumeta–Alcantara fault of Pliocene age (Ghisetti and Vezzani, 1984).

## 9. Conclusions

The Cretaceous karstified limestone in the Madonie Mountains has been identified as a potential reservoir unit in the Sicilian FTB. The porosity is secondary in nature and is related to karstification and limestone dissolution during emergence of the Panormide carbonate platform in the Cretaceous.

The fluid flow history in the karstified limestones was reconstructed, based on field, petrographic, geochemical and microthermometric data from diagenetic cements in the karst reservoir and in Pliocene high-angle faults in the study area. The fluid flow history has been subdivided into five stages. The transition from one stage to another is marked by important changes in the fluid composition and/or the physico-chemical conditions at which diagenetic precipitation took place. These changes have been linked to events in the kinematic and burial history, leading to a paragenesis that is linked to the absolute time scale. For example, infiltration of seawater in the karst cavities was dated with nannopalaeontology and $^{87}Sr/^{86}Sr$ isotope ratios. Another example regards the influx of high saline, hot and radiogenic fluids that could be linked to high-angle fault development along which similar fluids migrated and caused local dolomitization.

Finally, linking the paragenesis to the kinematic and burial history enabled us to constrain the timing of hydrocarbon migration in north-central Sicily. The latter is new information for the region and could spark renewed interest in the Sicilian fold and thrust belt as a prospective hydrocarbon province (Granath and Casero, 2004). From the results of the present study, it is clear, that maturation of the, at present, unknown source rock was only possible after foredeep and possibly also tectonic burial. This shows that hydrocarbon migration routes were most likely at large controlled by tectonic activity. The hydrocarbon migration in the study area has been related to expulsion from the north to the south during active tectonic compression in the Middle Miocene.

## Acknowledgements

The PhD research of the first author was financed by the Institute for the Promotion of Innovation through Science and Technology in Flanders (IWT-Vlaanderen). We are grateful to Prof. M. Joachimski from the University of Erlangen who kindly provided the stable isotope analyses. H. Nijs is kindly thanked for preparing the thin sections. V. Gallagher and A. Kelly are acknowledged for their practical help during $^{87}Sr/^{86}Sr$ isotope analysis at the SUERC.

## References

Aldega, L., Corrado, S., Grasso, M., Maniscalco, R., 2007. Correlation of diagenetic data from organic and inorganic studies in the Apenninic–Maghrebian fold-and-thrust belt: a case study from Eastern Sicily. The Journal of Geology 115, 335–353.

Allan, J.R., Matthews, R.K., 1982. Isotope signatures associated with early meteoric diagenesis. Sedimentology 29, 797–817.

Amthor, J.E., Friedman, G.M., 1992. Early- to late-diagenetic dolomitization of platform carbonates; Lower Ordovician Ellenburger Group, Permian Basin, West Texas. Journal of Sedimentary Research 62 (1), 131–144.

Anderson, R.K., Arthur, M.A., 1983. Stable isotopes of oxygen and carbon and their application to sedimentologic and paleoenvironmental problems. In: Arthur, M.A., Anderson, T.F., Kaplan, I.R., Veizer, J., Land, S. (Eds.), Stable Isotopes in Sedimentary Geology 10. SEPM Short Course, Columbia, pp. 1–151.

Andre, P., Doulcet, A., 1987. Rospo Mare karstified limestone oil-field. AAPG Bulletin 71 (5) 525–525.

Anelli, L., Mattavelli, L., Pieri, M., 1996. Structural-stratigraphic evolution of Italy and its petroleum systems. In: Ziegler, P.A., Horvath, F. (Eds.), Peri-Tethys Memoir 2: Structure and Prospects of Alpine Basins and Forelands, vol. 170. Museum Nationale d'Histoire Naturelle, Paris, pp. 15–45.

Bachu, S., 1997. Flow of formation waters, aquifer characteristics, and their relation to hydrocarbon accumulations, northern Alberta basin. AAPG Bulletin 81 (5), 712–733.

Badiozamani, K., 1973. The dorag dolomitization model – application to the middle Ordovician of Wisconsin. Journal of Sedimentary Petrology 43, 965–984.

Bello, M., Franchino, A., Merlini, S., 2000. Structural model of eastern Sicily. Memoria della Societa Geologica Italiana 55, 61–70.

Benchilla, L., Guilhaumou, N., Mougin, P., Jaswal, T., Roure, F., 2003. Reconstruction of palaeo-burial history and pore fluid pressure in foothill areas: a sensitivity test in the Hammam Zriba (Tunisia) and Koh-i-Maran (Pakistan) ore deposits. Geofluids 3 (2), 103–123.

Bodnar, R.J., 1993. Revised equation and table for determining the freezing-point depression of $H_2O$–NaCl solutions. Geochimica et Cosmochimica Acta 57 (3), 683–684.

Boles, J.R., Franks, S.G., 1979. Clay Diagenesis in Wilcox Sandstones of Southwest Texas - Implications of smectite diagenesis on Sandstone Cementation. Journal of Sedimentary Petrology 49 (1), 55–70.

Boni, M., 1986. The Permo-Triassic vein and paleokarst ores in southwest Sardinia – contribution of fluid inclusion studies to their genesis and paleoenvironment. Mineralium Deposita 21 (1), 53–62.

Bourque, P.-A., Savard, M.M., Chi, G., Dansereau, P., 2001. Diagenesis and porosity evolution of the Upper Silurian–lowermost Devonian West Point reef limestone, eastern Gaspé Belt, Québec Appalachians. Bulletin of Canadian Petroleum Geology 49 (2), 299–326.

Bradbury, H.J., Woodwell, G.R., 1987. Ancient fluid flow within foreland terrains. In: Goff, J.C., Williams, B.P.J. (Eds.), Fluid Flow in Sedimentary Basins and Aquifers, vol. 34. Geological Society of London, pp. 87–102.

Breesch, L., Swennen, R., Dewever, B., Mezini, A., 2007. Deposition and diagenesis of carbonate conglomerates in the Kremenara anticline, Albania: a paragenetic time marker in the Albanian foreland fold-and-thrust belt. Sedimentology 54 (1), 483–496.

Brocquet, P., 1970. The geology of the Madonie Mountains of Sicily. In: Alvarez, W., Gohrbandt, K.H.A. (Eds.), Geology and History of Sicily. Petroleum Exploration Society of Libya, Tripoli.

Burke, W.H., Denison, R.E., Hetherington, E.A., Koepnick, R.B., Nelson, H.F., Otto, J.B., 1982. Variation of Sea-Water $^{87}Sr/^{86}Sr$ throughout Phanerozoic Time. Geology 10 (10), 516–519.

Burruss, R.C., 1991. Practical aspects of fluorescence microscopy of petroleum fluid inclusions. In: Barker, C., Kopp, O.C. (Eds.), Luminescence Microscopy and Spectroscopy: Qualitative and Quantitative Applications, vol. 25. SEPM Short Course, pp. 1–7.

Catalano, R., Marniaci, G., Renda, P., Viso, G., 1973. Un esempio di evoluzione di bacino dei Monti di Palermo, la successione Mesozoico-Terziaria di Cala Rossa (Terrassini). Geologica Romana 12, 151–175.

Catalano, R., Di Stefano, P., Sulli, A., Vitale, F.P., 1996. Paleogeography and structure of the central Mediterranean: Sicily and its offshore area. Tectonophysics 260 (4), 291–323.

Catalano, R., Franchino, A., Merlini, S., 2000. Central western Sicily structural setting interpreted from seismic reflection profiles. Memoria della Societa Geologica Italiana 55, 5–16.

Connolly, C.A., Walter, L.M., Baadsgaard, H., Longstaffe, F.J., 1990. Origin and evolution of formation waters, Alberta Basin, Western Canada sedimentary basin (2) isotope systematics and water mixing. Applied Geochemistry 5 (4), 397–413.

Crane, R.C., 1990. Exploration techniques in thrust belts. Memoria della Societa Geologica Italiana 45, 815–816.

Dahlmann, A., de Lange, G.J., 2003. Fluid-sediment interactions at Eastern Mediterranean mud volcanoes: a stable isotope study from ODP Leg 160. Earth and Planetary Science Letters 212 (3–4), 377–391.

Del Ben, A., Guarnieri, P., 2000. Neogene transpression in the Cefalu Basin (Southern Tyrrhenian): comparison between land and marine data. Memoria della Societa Geologica Italiana 55, 27–33.

Dewever, B., Swennen, R., Cooreman, M., 2006. Fluid flow in the Sicilian accretionary wedge: primary geochemical signatures or recrystallization mask. Journal of Geochemical Exploration 89 (1–3), 83–86.

Di Stefano, P., Alessi, A., Gullo, M., 1996. Mesozoic and Paleogene megabreccias in southern Sicily: new data on the Triassic paleomargin of the Siculo-Tunisian platform. Facies 34, 101–122.
Di Stefano, P., Ruberti, D., 2000. Cenomanian Rudist-dominated Shelf margin Limestones from the Panormide carbonate platform (Sicily, Italy): facies analysis and sequence stratigraphy. Facies 42, 133–160.
Di Stefano, P., Galacz, A., Mallarino, G., Mindszenty, A., Voros, A., 2002. Birth and early evolution of a Jurassic escarpment: Monte Kumeta, Western Sicily. Facies 46, 273–298.
Dia, A.N., Castrec, M., Boulegue, J., Boudou, J.P., 1995. Major and trace-element and Sr isotope constraints on fluid circulations in the Barbados accretionary complex 1. Fluid Origin. Earth and Planetary Science Letters 134 (1–2), 69–85.
Dickson, J.A.D., 1966. Carbonate identification and genesis as revealed by staining. Journal of Sedimentary Petrology 36, 491–505.
Elter, P., Grasso, M., Parotto, M., Vezzani, L., 2003. Structural setting of the Apennine–Maghrebian thrust belt. Episodes 26 (3), 205–211.
Favara, R., Grassa, F., Inguaggiato, S., D'Amore, F., 1998. Geochemical and hydrogeological characterization of thermal springs in Western Sicily, Italy. Journal of Volcanology and Geothermal Research 84 (1-2), 125–141.
Ferket, H., Swennen, R., Ortuño-Arzate, S., Cacas, M.C., Roure, F., 2004. Hydrofracturing in the Laramide foreland fold-and-thrust belt of Eastern Mexico. In: Swennen, R., Roure, F., Granath, J. (Eds.), Deformation, Fluid Flow and Reservoir Appraisal in Foreland Fold-and-thrust Belts, vol. 1. AAPG Hedberg Memoir, pp. 133–156.
Friedman, I., O'Neil, J.R. 1977. Compilation of stable isotope fractionation factors of geochemical interest. United States Geological Survey Professional Paper 440.
Gasparrini, M., Bechstadt, T., Boni, M., 2006. Massive hydrothermal dolomites in the southwestern Cantabrian Zone (Spain) and their relation to the Late Variscan evolution. Marine and Petroleum Geology 23 (5), 543–568.
Ghisetti, F., Vezzani, L., 1984. Thin-skinned deformations of the Western Sicily thrust belt and relationships with crustal shortening: mesostructural data on the Mt. Kumeta–Alcantara fault zone and related structures. Bolletino della Societa Geologica Italiana 103, 129–157.
Giunta, G., Nigro, F., Renda, P., 2000a. Extensional tectonics during Maghrebides chain building since late Miocene: examples from Northern Sicily. Annales Societatis Geologrum Poloniae 70, 81–98.
Giunta, G., Nigro, F., Renda, P., Giorgianni, A., 2000b. The Sicilian–Maghrebian Tyrrhenian margin: a neotectonic evolutionary model. Bolletino della Societa Geologica Italiana 119, 553–565.
Goldstein, R.H., Reynolds, T.J., 1994. Systematics of Fluid Inclusions in Diagenetic Minerals, vol. 31. SEPM Short Course, Tulsa, 198 p.
Granath, J., Casero, P., 2004. Tectonic setting of the petroleum systems of Sicily. In: Swennen, R., Roure, F., Granath, J. (Eds.), Deformation, Fluid Flow and Reservoir Appraisal in Foreland Fold and Thrust Belts, vol. 1. AAPG Hedberg Memoir, pp. 391–411.
Johansson, M., Braakenburg, N.E., Stow, D.A.V., Faugères, J.-C., 1998. Deep-water massive sands: facies, processes and channel geometry in the Numidian Flysch, Sicily. Sedimentary Geology 115, 233–265.
Jolivet, L., Faccenna, C., 2000. Mediterranean extension and the Africa–Eurasia collision. Tectonics 19 (6), 1095–1106.
Kastner, M., Le Pichon, X., 1992. Fluids in convergent margins. Earth and Planetary Science Letters 109, 275–504.
Kerans, C., 1988. Karst-controlled reservoir heterogeneity in Ellenburger Group carbonates of West Texas. American Association of Petroleum Geologists Bulletin 72 (10), 1160–1183.
Land, L.S., 1980. The isotopic and trace element geochemistry of dolomite: the state of the art. In: Zenger, D.H., Dunham, J.B. (Eds.), Concepts and models of dolomitization. Special publication of the Society of economic paleontologists and mineralogists 28. Society of economic paleontologists and mineralogists, Tulsa, pp. 87–110.
Larroque, C., Guilhaumou, N., Stephan, J.-F., Roure, F., 1996. Advection of fluids at the front of the Sicilian Neogene subduction complex. Tectonophysics 254, 41–55.
Lentini, F., Vezzani, L. 1974. Carta geologica delle Madonie (Sicilia Centro-Settentrionale).
Lohmann, K.C., 1988. Geochemical patterns of meteoric diagenetic systems and their application to studies of paleokarst. In: James, N.P., Choquette, P.W. (Eds.), Paleokarst. Springer-Verlag, New York, pp. 58–80.
Mabhoubi, A., Moussavi-Harami, R., Brenner, R.L., Gonzalez, L.A., 2002. Diagenetic history of Late Palaeocene potential carbonate reservoir rocks, Kopet-Dagh Basin, NE Iran. Journal of Petroleum Geology 25 (4), 465–484.
Machel, H.G., Burton, E.A., 1991. Factors governing cathodoluminescence in calcite and dolomite, and their implications for studies of carbonate diagenesis. In: Barker, C., Kopp, O.C. (Eds.), Luminescence Microscopy and Spectroscopy: Qualitative and Quantitative Applications. SEPM Short Course 25. Society of Economic Paleontologists and Mineralogists, Tulsa, pp. 9–25.
Machel, H.G., Cavell, P.A., 1999. Low-flux, tectonically-induced squeegee fluid flow (“hot flash”) into the Rocky Mountain foreland basin. Bulletin of Canadian Petroleum Geology 47 (4), 510–533.
Mascle, A., Vially, R., Deville, E., BijuDuval, B., Roy, J.P., 1996. The petroleum evaluation of a tectonically complex area: the western margin of the Southeast Basin (France). Marine and Petroleum Geology 13 (8), 941–961.
McArthur, J.M., Howarth, R.J., Bailey, T.R., 2001. Strontium isotope stratigraphy: Lowess Version 3: Best Fit to the Marine Sr-isotope curve for 0–509 Ma and accompanying look-up table for deriving numerical age. Journal of Geology 109, 155–170.
McCaig, A.M., Tritlla, J., Banks, D.A., 2000. Fluid mixing and recycling during Pyrenean thrusting: evidence from fluid inclusion halogen ratios. Geochimica et Cosmochimica Acta 64 (19), 3395–3412.
Min, M.Z., Wu, J.Q., 1998. Stable isotope studies of paleokarst-hosted uranium deposits in China. Geochemical Journal 32 (2), 103–115.
Miuccio, G., Frixa, A., Bertamoni, M., 2000. The Trapanese structural domain in the Termini Imerese Mountain area (Sicily). Memoria della Societa Geologica Italiana 55, 227–234.
Moore, C.H., 2001. Carbonate Reservoirs: Porosity Evolution and Diagenesis in a Sequence Stratigraphic Framework. Elsevier, Amsterdam, 444 p.
Moore, J.C., Vrolijk, P., 1992. Fluids in accretionary prisms. Reviews of Geophysics 30 (2), 113–135.
Moretti, I., Labaume, P., Sheppard, S.M.F., Boulegue, J., 2002. Compartmentalisation of fluid migration pathways in the sub-Andean Zone, Bolivia. Tectonophysics 348 (1–3), 5–24.
Morrow, D.W., 1982. Descriptive field classification of sedimentary and diagenetic breccia fabrics in carbonate rocks. Bulletin of Canadian Petroleum Geology 30 (3), 227–229.
Naden, J. 1993. Calcicbrine 1.5: a Microsoft Excel 5.0 Add-in for Calculation Salinities from Microthermometric Data in the System $NaCl–CaCl_2–H_2O$. Abstracts of PACROF VI Wisconsin.
Nigro, F., Renda, P., 2000. Un modello di evoluzione tettono-sedimentaria dell'avanfossa neogenica siciliana. Bolletino della Societa Geologica Italiana 119, 667–686.
Nigro, F., Renda, P., 2002. From Mesozoic extension to Tertiary collision: deformation patterns in the units of the North-Western Sicilian chain. Bolletino della Societa Geologica Italiana 121, 87–97.
Oliver, J., 1986. Fluids expelled tectonically from orogenic belts: their role in hydrocarbon migration and other geologic phenomena. Geology 14, 99–102.
O'Neil, J.R., Epstein, S., 1969. Oxygen isotope fractionation in the system dolomite-calcite-carbon dioxide. Science 152, 198–200.
Railsback, L.B., Brook, G.A., Chen, J., Kalin, R., Fleischer, C.J., 1994. Environmental controls on the petrology of a Late Holocene speleothem from Botswana with annual layers of calcite and aragonite. Journal of Sedimentary Research section A – Sedimentary Petrology and Processes 64, 147–155.
Rosenbaum, G., Lister, G.S., Duboz, C., 2002. Reconstruction of the tectonic evolution of the western Mediterranean since the Oligocene. In: Rosenbaum, G., Lister, G.S. (Eds.), Reconstruction of the evolution of the Alpine-Himalayan Orogen. Journal of The virtual explorers, 8, pp. 107–126.
Rosenbaum, G., Lister, G.S., 2004a. Formation of arcuate orogenic belts in the western Mediterranean region. Geological Society of America Special Paper 383, 41–56.
Rosenbaum, G., Lister, G.S., 2004b. Neogene and Quaternary rollback evolution of the Tyrrhenian Sea, the Apennines, and the Sicilian Maghrebides. Tectonics 23 (1), TC1013. doi:10.1029/2003TC001518.
Roure, F., Howell, D.G., Muller, C., Moretti, I., 1990. Late Cenozoic subduction complex of Sicily. Journal of Structural Geology 12 (2), 259–266.
Roure, F., Nazaj, S., Mushka, K., Fili, I., Cadet, J.-P., Bonneau, M., 2004. Kinematic evolution and petroleum systems: an appraisal of the Outer Albanides. AAPG – Memoir Thrust Tectonics and Hydrocarbon Systems 82, 474–493.
Roure, F., Swennen, R., Schneider, F., Faure, J.L., Ferket, H., Guilhaumou, N., Osadetz, K., Robion, P., Vandeginste, V., 2005. Incidence of tectonics and natural fluid migration on reservoir evolution in foreland fold and thrust belts. Revue de l'IFP 60 (1), 67–107.
Schneider, F., 2003. Basin modelling in complex area: examples from eastern Venezuelan and Canadian foothills. Oil and Gas Science and Technology – Revue de l'institut Francais du Petrole 58 (2), 313–324.
Searl, A., 1989. Saddle dolomite – a new view of its nature and origin. Mineralogical Magazine 53 (373), 547–555.
Sheppard, S.M.F., 1986. Characterization and isotopic variations in natural waters. In: Valley, J.W., Taylor, H.P., O'Neil, J. (Eds.), Stable Isotopes in High Temperature Geological Processes. Mineralogical society of America, Washington, pp. 165–181.
Sibley, D.F., Gregg, J.M., 1987. Classification of dolomite rock textures. Journal of Sedimentary Petrology 57 (6), 967–975.
Soudet, H.J., Sorriaux, P., Rolando, J.P., 1994. Relationship between fractures and karstification – the oil-bearing paleokarst of Rospo Mare (Italy). Bulletin Des Centres De Recherches Exploration-Production Elf Aquitaine 18 (1), 257–297.
Stampfli, G.M., Borel, G.D., 2002. A plate tectonic model for the Paleozoic and Mesozoic constrained by dynamic plate boundaries and restored synthetic oceanic isochrons. Earth and Planetary Science Letters 196 (1–2), 17–33.
Stueber, A., Pushkar, P., Hetherington, E.A., 1984. A strontium isotopic study of Smackover brines and associated solids, southern Arkansas. Geochimica et Cosmochimica Acta 48, 1637–1649.
Swennen, R., Roure, F., Granath, J., 2004. Deformation History, Fluid Flow Reconstruction and Reservoir Appraisal in Foreland Fold and Thrust Belts. AAPG Hedberg Memoir vol. 1, 430 p.
Taylor, T.R., 1990. The influence of calcite dissolution on reservoir porosity in Miocene sandstones, Picaroon Field, offshore Texas Gulf-Coast. Journal of Sedimentary Petrology 60 (3), 322–334.
Travé, A., Calvet, F., 2001. Syn-rift geofluids in fractures related to the early–middle Miocene evolution of the Valle's-Penede's half-graben (NE Spain). Tectonophysics 336 (1–4), 101–120.
Travé, A., Calvet, F., Soler, A., Labaume, P., 1998. Fracturing and fluid migration during Palaeogene compression and Neogene extension in the Catalan Coastal Ranges, Spain. Sedimentology 45, 1063–1082.

Valenza, K., Moritz, R., Mouttaqi, A., Fontignie, D., Sharp, Z., 2000. Vein and karst barite deposits in the Western Jebilet of Morocco: fluid inclusion and isotope (S, O, Sr) evidence for regional fluid mixing related to Central Atlantic rifting. Economic Geology 95, 587–606.

Van Geet, M., Swennen, R., Durmishi, C., Roure, F., Muchez, P., 2002. Paragenesis of Cretaceous to Eocene carbonate reservoirs in the Ionian fold and thrust belt (Albania): relation between tectonism and fluid flow. Sedimentology 49 (4), 697–718.

Vandeginste, V., Swennen, R., Gleeson, S.A., Ellam, R.M., Osadets, K., Roure, F., 2005. Zebra dolomitization as a result of focused fluid flow in the Rocky Mountains Fold and Thrust Belt, Canada. Sedimentology 52 (5), 1067–1095.

Veizer, J., Ala, D., Azmy, K., Bruckschen, P., Buhl, D., Bruhn, F., Carden, G.A.F., Diener, A., Ebneth, S., Godderis, Y., Jasper, T., Korte, G., Pawellek, F., Podlaha, O.G., Strauss, H., 1999. Sr-87/Sr-86, delta C-13 and delta O-18 evolution of Phanerozoic seawater. Chemical Geology 161 (1–3), 59–88.

Voigt, S., Wilmsen, M., Mortimore, R.M., Voigt, T., 2003. Cenomanian palaeotemperatures derived from the oxygen isotopic composition of brachiopods and belemnites: evaluation of Cretaceous palaeotemperature proxies. International Journal of Earth Sciences 92, 285–299.

Wachter, E.A., Hayes, J.M., 1985. Exchange of oxygen isotopes in carbon dioxide–phosphoric acid systems. Chemical Geology 52 (3–4), 365–374.

Wagner, P.D., 1990. Geochemical stratigraphy and porosity controls in Cretaceous carbonates near the Oman Mountains. In: Evolution of the Oman Tethyan Continental Margin. Geological Society of London, vol. 49. Special Publications, pp. 127–137.

Warren, J., 2000. Dolomite: occurrence, evolution and economically important associations. Earth-Science Reviews 52 (1–3), 1–81.